

---

---

# **TASK 6: Suppression Pool Void Distribution During Blowdown**

**Scaling, Overall Dimensions, Proposed Test Facility  
Modifications, and Instrumentation**

---

---

Prepared by

M. Ishii, T. Hibiki, S. Rassame, D. Y. Lee, J. Yang, and S. W. Choi

Prepared for

U.S. Nuclear Regulatory Commission

**September 2009**





## TABLE OF CONTENTS

	Page
LIST OF TABLES .....	iv
LIST OF FIGURES .....	v
CHAPTER 1. INTRODUCTION .....	1
1.1. Research Background .....	1
1.2. Research Objective .....	5
1.3. PUMA-E Facility .....	5
1.4. MARK-I Containment .....	8
CHAPTER 2. SCALING CONSIDERATION.....	10
2.1. Basis of Scaling Approach.....	10
2.2. Scaling for Facility Modification.....	14
2.3. Demonstration of Scaling Approach.....	17
CHAPTER 3. FACILITY MODIFICATION.....	40
3.1. Facility Modification for Steady-State Tests .....	40
3.1.1. Air Injection System for Steady-State Tests .....	40
3.1.2. Downcomer Section for Steady-State Tests.....	43
3.2. Facility Modification for Transient Tests .....	46
CHAPTER 4. INSTRUMENTATIONS.....	50
4.1. Local Instruments in SP .....	50
4.1.1. Conductivity Probes and Supporting Cage .....	50
4.1.2. Single-Sensor Conductivity Probes in Downcomer.....	54
4.1.3. Thermocouples on Cage.....	54
4.1.4. Pressure, Temperature and Water Level Measurement in SP.....	55
4.1.5. Air Concentration Measurement.....	56
4.2. Instruments outside SP.....	58
4.2.1. Instruments in Air Injection Line.....	58
4.2.1.1. Vortex Flow Meter.....	58
4.2.1.2. Pressure and Temperature.....	58
4.2.2. High-Speed Video Movie Camera.....	59
4.2.3. Existing Instruments in PUMA-E Facility.....	59
4.2.3.1. Flow Measurement.....	59
4.2.3.2. Pressure and Temperature Measurement in DW .....	59
CHAPTER 5. SUMMARY AND FUTURE WORK .....	61
LIST OF REFERENCES.....	62

## LIST OF TABLES

Table	Page
Table 1.1 PUMA-E Facility Key Parameters [3].....	7
Table 1.2 MARK-I Key Parameters [5].....	9
Table 2.1 Comparison between MARK-I and PUMA-E.....	13
Table 2.2 Scaling for Steady-State Tests .....	15
Table 2.3 Scaling for Transient Tests .....	16
Table 2.4 Inlet Boundary Conditions Suggested by NRC [6] .....	20
Table 2.5 Details of CFD Simulation .....	20

## LIST OF FIGURES

Figure	Page
Figure 1.1 Local Phenomena in SP during Blowdown Period of Air Injection. ....	3
Figure 1.2 Local Phenomena in SP during Blowdown Period of Steam-Air .....	4
Figure 1.3 Schematic of PUMA facility. ....	7
Figure 1.4 Venting System and Suppression Chamber of the MARK-I [4]. ....	9
Figure 2.1 Schematic of Water Column after Vent Clearing.....	13
Figure 2.2 SP Geometries for MARK-I and PUMA-E to Perform CFD Simulation. ....	21
Figure 2.3 Inlet Boundary Condition Applied to MARK-I .....	22
Figure 2.4 Inlet Boundary Condition Applied to PUMA-E.....	23
Figure 2.5 Void Distribution with Time (MARK-I and PUMA-E 3” Downcomer, $\tau_{vc}=0.34$ second, $0.0\tau_{vc} \leq t \leq 1.0\tau_{vc}$ ). ....	24
Figure 2.6 Void Distribution with Time (MARK-I and PUMA-E 3” Downcomer, $\tau_{vc}=0.34$ second, $1.25\tau_{vc} \leq t \leq 2.25\tau_{vc}$ ). ....	25
Figure 2.7 Void Distribution with Time (MARK-I and PUMA-E 3” Downcomer, $\tau_{vc}=0.34$ second, $2.5\tau_{vc} \leq t \leq 3.25\tau_{vc}$ ). ....	26
Figure 2.8 Void Distribution with Time (MARK-I and PUMA-E 3” Downcomer, $\tau_{vc}=0.34$ second, $3.5\tau_{vc} \leq t \leq 6.0\tau_{vc}$ ). ....	27
Figure 2.9 Axial Liquid Velocity Distribution (MARK-I and PUMA-E 3” Downcomer, $\tau_{vc}=0.34$ second, $t = 0.5\tau_{vc}$ ). ....	28
Figure 2.10 Radial Liquid Velocity Distribution (MARK-I and PUMA-E 3” Downcomer, $\tau_{vc}=0.34$ second, $t = 0.5\tau_{vc}$ ). ....	28
Figure 2.11 Local Axial and Radial Liquid Velocity Distributions (MARK-I and PUMA- E 3” Downcomer, $\tau_{vc}=0.34$ second, $t = 0.5\tau_{vc}$ ). ....	29
Figure 2.12 Axial Liquid Velocity Distribution (MARK-I and PUMA-E 3” Downcomer, $\tau_{vc}=0.34$ second, $t = 1.0\tau_{vc}$ ). ....	30
Figure 2.13 Radial Liquid Velocity Distribution (MARK-I and PUMA-E 3” Downcomer, $\tau_{vc}=0.34$ second, $t = 1.0\tau_{vc}$ ). ....	30
Figure 2.14 Local Axial and Radial Liquid Velocity Distributions (MARK-I and PUMA- E 3” Downcomer, $\tau_{vc}=0.34$ second, $t = 1.0\tau_{vc}$ ). ....	31
Figure 2.15 Axial Liquid Velocity Distribution (MARK-I and PUMA-E 3” Downcomer, $\tau_{vc}=0.34$ second, $t = 1.5\tau_{vc}$ ). ....	32
Figure 2.16 Radial Liquid Velocity Distribution (MARK-I and PUMA-E 3” Downcomer, $\tau_{vc}=0.34$ second, $t = 1.5\tau_{vc}$ ). ....	32

Figure 2.17 Local Axial and Radial Liquid Velocity Distributions (MARK-I and PUMA-E 3” Downcomer, $\tau_{vc}=0.34$ second, $t = 1.5\tau_{vc}$ ).....	33
Figure 2.18 Axial Liquid Velocity Distribution (MARK-I and PUMA-E 3” Downcomer, $\tau_{vc}=0.34$ second, $t = 2.5\tau_{vc}$ ).....	34
Figure 2.19 Radial Liquid Velocity Distribution (MARK-I and PUMA-E 3” Downcomer, $\tau_{vc}=0.34$ second, $t = 2.5\tau_{vc}$ ).....	34
Figure 2.20 Local Axial and Radial Liquid Velocity Distributions (MARK-I and PUMA-E 3” Downcomer, $\tau_{vc}=0.34$ second, $t = 2.5\tau_{vc}$ ).....	35
Figure 2.21 Axial Liquid Velocity Distribution (MARK-I and PUMA-E 3” Downcomer, $\tau_{vc}=0.34$ second, $t = 4.0\tau_{vc}$ ).....	36
Figure 2.22 Radial Liquid Velocity Distribution (MARK-I and PUMA-E 3” Downcomer, $\tau_{vc}=0.34$ second, $t = 4.0\tau_{vc}$ ).....	36
Figure 2.23 Local Axial and Radial Liquid Velocity Distributions (MARK-I and PUMA-E 3” Downcomer, $\tau_{vc}=0.34$ second, $t = 4.0\tau_{vc}$ ).....	37
Figure 2.24 Axial Liquid Velocity Distribution (MARK-I and PUMA-E 3” Downcomer, $\tau_{vc}=0.34$ second, $t = 6.0\tau_{vc}$ ).....	38
Figure 2.25 Radial Liquid Velocity Distribution (MARK-I and PUMA-E 3” Downcomer, $\tau_{vc}=0.34$ second, $t = 6.0\tau_{vc}$ ).....	38
Figure 2.26 Local Axial and Radial Liquid Velocity Distributions (MARK-I and PUMA-E 3” Downcomer, $\tau_{vc}=0.34$ second, $t = 6.0\tau_{vc}$ ).....	39
Figure 3.1 Experimental Facility for Steady-State Tests.....	42
Figure 3.2 Side View of SP with Modification for Steady-State Tests.....	44
Figure 3.3 Top View of SP with Modification for Steady-State Tests.....	45
Figure 3.4 Experimental Facility for Transient Tests.....	47
Figure 3.5 Side View of SP with Modification for Transient Tests.....	48
Figure 3.6 Top View of SP with Modification for Transient Tests.....	49
Figure 4.1 Design of Single-Sensor Conductivity Probe.....	52
Figure 4.2 Design of Double-Sensor Conductivity Probe.....	52
Figure 4.3 Configuration of Single-Sensor and Double-Sensor Conductivity Probes.....	53
Figure 4.4 Configuration of the Single-Sensor Conductivity Probes in Downcomer.....	54
Figure 4.5 Locations of Pressure and Water Level Measurement in SP.....	55
Figure 4.6 Oxygen Sampling Line inside SP.....	57
Figure 4.7 DW Pressure and Level Transmitter Locations.....	60

## CHAPTER 1. INTRODUCTION

### 1.1. Research Background

The possible failure of the low pressure Emergency Core Cooling System (ECCS) due to a large amount of entrained gas into the ECCS suction piping of a BWR is addressed in the Generic Safety Issue (GSI) 193, BWR ECCS suction concerns. Furthermore, air ingestion over 15% to the Residual Heat Removal (RHR) and containment spray pumps can fully degrade the pump performance [1]. Therefore, it is important to understand the dynamics of the Drywell (DW) to Suppression Pool (SP) venting phenomena during blowdown and the void distribution where the strainers are located. The void distribution, bubble size, and rate of jet spread are the key parameters in the analysis of the physical phenomena.

The void distribution in the SP during the blowdown period of a design basis accident is affected by several important local phenomena. In the initial blowdown, the steam and superheated water are released into the DW. As a result, pressure in the DW and downcomers in the SP increase rapidly. At the early stage of the blowdown, mostly noncondensable gas is forced through downcomers into the SP [2]. This is followed by the steam-air mixture injection. In the later stage, mostly steam is vented. The water initially standing in the downcomers is accelerated into the SP and the downcomers are voided. Then a large air bubble is formed at the exit of the downcomer. The air injection from the DW results in the expansion of this bubble at the tip of the downcomer. After that, this large bubble may deform and smaller disintegrated bubbles spread and rise to the water surface. Figure 1.1 schematizes local phenomena in the SP during the blowdown period of air injection. During the air injection phase, it is noted that some disintegrated bubbles may be entrained into the bottom of the pool due to the circulating

liquid flow. When the steam-air mixtures come into the downcomers, condensation occurs at the exit of the downcomers. This induces the chugging phenomenon at the exit of the downcomers with the rapid condensation. Figure 1.2 shows the local phenomena in the SP during the blowdown period of steam-air mixtures injection.

Both the steady-state and transient tests using the PUMA-E facility are proposed in order to study the local phenomena in the SP. In the steady-state tests, the different air mass flows are injected into the downcomers as boundary conditions. For the transient tests, the actual blowdown period in the DW and subsequent injection of sequential flows of the air, steam-air mixtures and pure steam are simulated by using the Reactor Pressure Vessel (RPV), DW and SP of the PUMA-E facility.

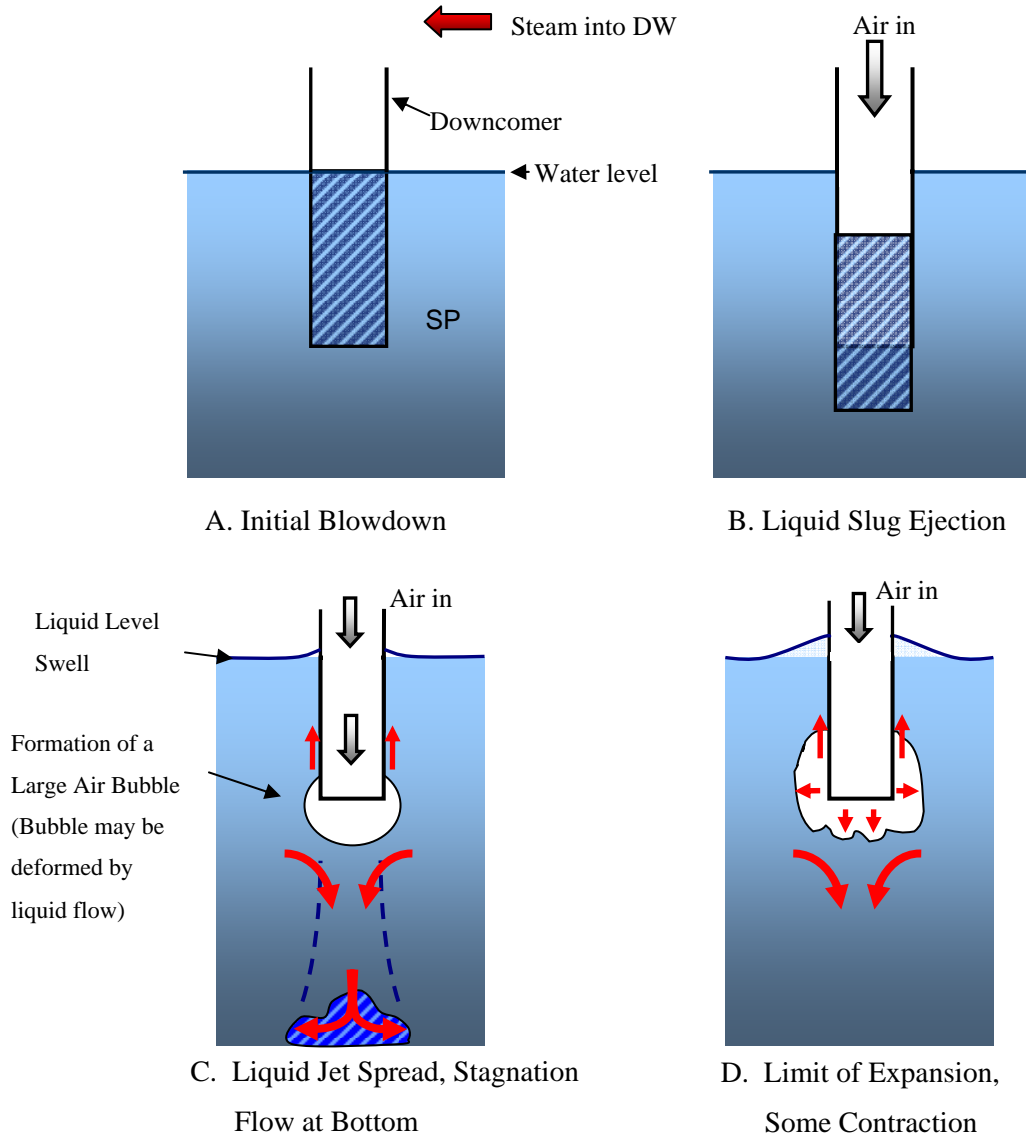
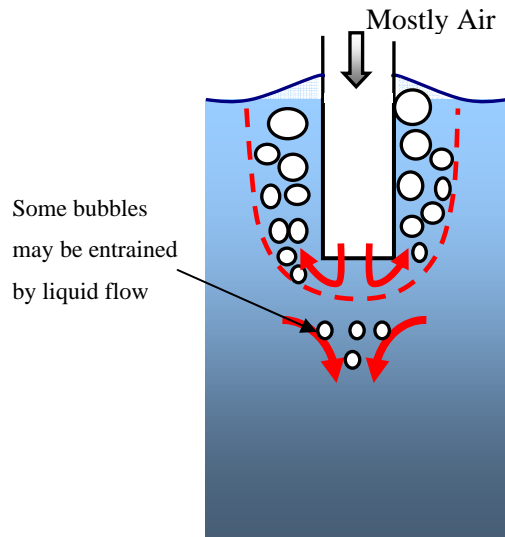
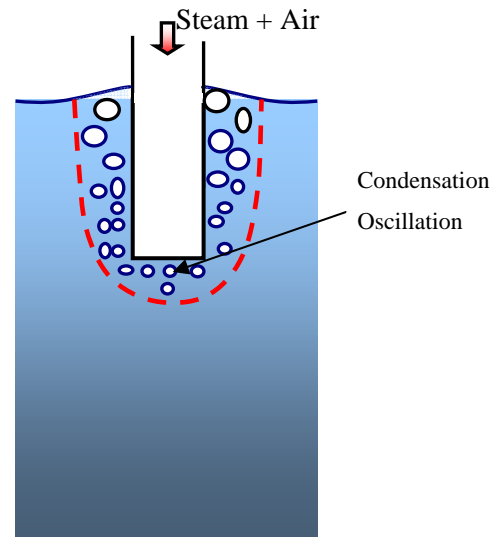


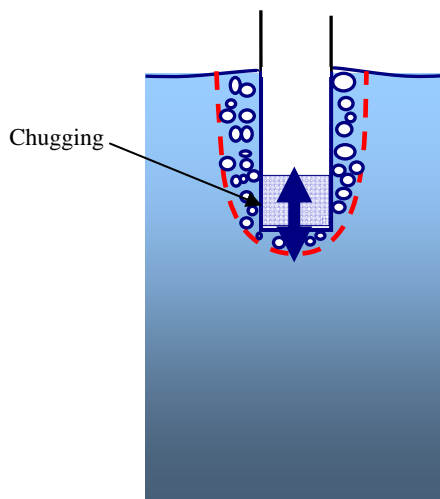
Figure 1.1 Local Phenomena in SP during Blowdown Period of Air Injection.



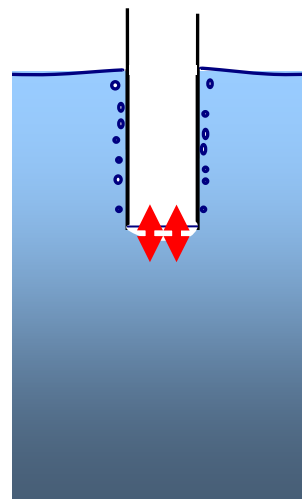
E. Bubble Disintegration, Formation



F. Concentration of Steam



G. Decrease of Air Flow (Bubbles) Chugging & Re-entry of Water



H. Rapid Condensation at Exit

Figure 1.2 Local Phenomena in SP during Blowdown Period of Steam-Air Mixtures Injection.

## 1.2. Research Objective

The primary objective of this study is to develop physical understanding and to obtain experimental data for the void distribution and fluid dynamics of the BWR SP during the blowdown period of LOCAs. Measurements of local void fraction and visual high speed movie recordings will be used to determine the break-up length of a downward jet containing steam and noncondensable gas. Measurements of the local void fraction give the rate at which the jet spreads, such that it is possible to estimate the void fraction and bubble size near the entrance of a strainer. The sensitivity of results to the noncondensable gas fraction is to be investigated.

Specific objectives are:

- To simulate the blowdown period of LOCAs using the modified PUMA-E facility so that void distribution tests in the SP can be conducted.
- To obtain a series of test data that covers a range of injection flow rates and noncondensable gas fraction for the blowdown conditions to determine local void fraction, bubble size and bubble velocity with a special focus on the locations where strainers for the ECCS suction are generally positioned.

## 1.3. PUMA-E Facility

The PUMA (Purdue University Multi-Dimensional Integral Test Assembly) facility was originally built to simulate the SBWR (Simplified Boiling Water Reactor) in terms of integral test performance and control. The project was sponsored by the U.S. Nuclear Regulatory Commission (NRC). The PUMA facility is an integral test facility including major components similar to the SBWR power plant, such as the Reactor Pressure Vessel (RPV), DW, Wetwell (WW), Gravity Driven Cooling System (GDCCS), Passive Containment Cooling System (PCCS), Isolation Condenser System (ICS), and

Automatic Depressurization System (ADS). The schematic of PUMA facility is shown in Figure 1.3.

The PUMA-E facility was modified from the PUMA facility to adapt the design changes from the SBWR to Economic Simplified Boiling Water Reactor (ESBWR). The heater rod, ADS, GDCS, PCCS and ICS have been modified based on the scaling and scientific design study for the ESBWR relative to the PUMA facility. The RPV, DW and WW geometries are identical to the PUMA facility. The WW is composed of gas space and SP which is water space. The details of the PUMA-E RPV, DW and WW can be found in the scientific design report for the PUMA facility [3]. Table 1.1 lists the important facility parameters.

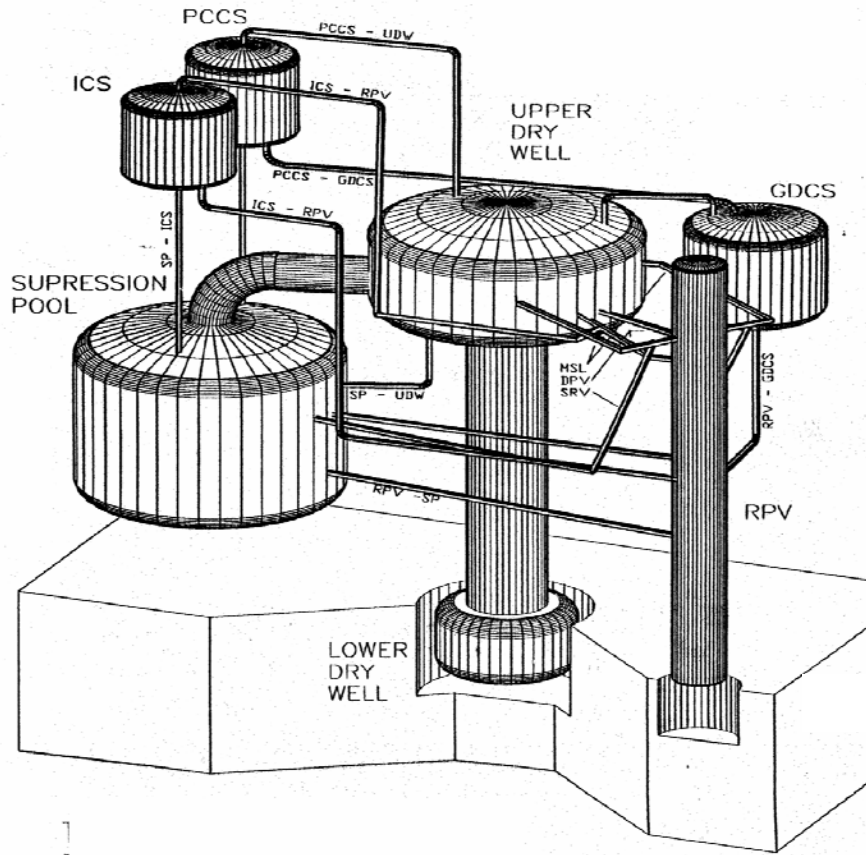


Figure 1.3 Schematic of PUMA facility.

Table 1.1 PUMA-E Facility Key Parameters [3]

Parameters	Value
Maximum Power (MWt)	630
RPV height / diameter (m)	6.126/0.6
RPV Free Volume (m <sup>3</sup> )	1.654
DW Free Volume (m <sup>3</sup> )	12.932
WW Water Volume (m <sup>3</sup> )	8.05
WW Gas Volume (m <sup>3</sup> )	9.63

#### 1.4. MARK-I Containment

The MARK-I containment functions in condensing steam released during LOCAs and provides a water source for the ECCS. The main components of the MARK-I containment are a drywell enclosed reactor vessel, torus-shaped suppression pool contained a large amount of water and venting system connecting the drywell and water space in the suppression pool [4].

Figure 1.4 shows the configuration of the venting system and suppression chamber of the MARK-I containment. 8 to 10 main vents connect the gas space of the drywell to the ring of vent headers. The ring of vent headers is linked by several downcomer pipes to the water space in suppression chamber. Table 1.2 lists important MARK-I parameters.

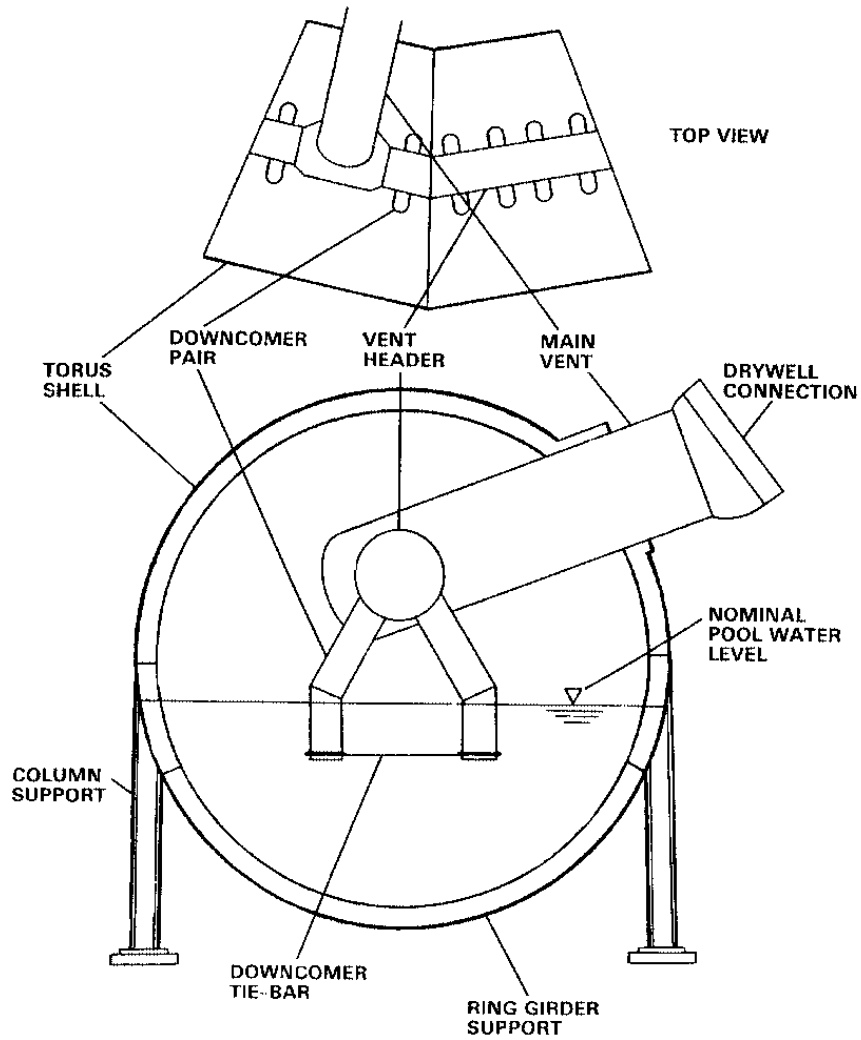


Figure 1.4 Venting System and Suppression Chamber of the MARK-I [4].

Table 1.2 MARK-I Key Parameters [5]

Parameter	Value
Maximum Power (MWt)	3,300
Drywell Free Volume (m <sup>3</sup> )	4,142
WetWell Water Volume (m <sup>3</sup> )	2,453.7
WetWell Gas Volume (m <sup>3</sup> )	3,148.8

## CHAPTER 2. SCALING CONSIDERATION

### 2.1. Basis of Scaling Approach

In order to study the venting phenomena of the BWR SP during the blowdown using the PUMA-E facility, proper scaling from the prototype to PUMA-E is necessary. The MARK-I SP is considered as the prototype facility. Table 2.1 shows the comparison of the power, dimensions of the DW and Wetwell and flow rate in a downcomer during blowdown between the MARK-I and PUMA-E facility.

Various ratios of the prototype over model can be defined as follows. The time ratio is given as

$$\tau_R = \tau_m / \tau_p, \quad (2-1)$$

the length ratio is defined as

$$L_R = L_m / L_p, \quad (2-2)$$

the diameter ratio is defined as

$$D_R = D_m / D_p, \quad (2-3)$$

the area ratio is defined as

$$A_R = A_m / A_p, \quad (2-4)$$

and the mass flow rate ratio is defined as

$$\dot{m}_R = \dot{m}_m / \dot{m}_p \quad (2-5)$$

where subscripts  $m$ ,  $p$  and  $R$  are the model, prototype and ratio between the model and prototype, respectively. Another important parameter is the vent clearing time as

$$\tau_{vc} \quad (2-6)$$

The non-dimensional height is defined as

$$z^* = z/H \quad (2-7)$$

where  $H$  is the height from SP bottom to downcomer exit. The non-dimensional radius is defined as

$$r^* = r/R \quad (2-8)$$

where  $R$  is the radius of downcomer.

To investigate the venting phenomena in the SP during the blowdown, real time scaling and pressure as well as fluid properties are assumed to be same between the prototype and PUMA-E. Thus, the time ratio is given as

$$\tau_R = 1, \quad (2-9)$$

the inlet velocity ratio is given as

$$v_{z,R} = L_R / \tau_R = L_R, \quad (2-10)$$

and the mass flow rate ratio is given as

$$m_R = \frac{\dot{m}_m}{\dot{m}_p} = \frac{\rho A_m v_{z,m}}{\rho A_p v_{z,p}} = A_R \cdot L_R \quad (2-11)$$

Equation (2-10) indicates that the inlet velocity as an inlet boundary condition can be scaled by the length ratio.

On the other hand, the liquid velocity distribution inside the SP is also an important parameter for entrainment of air bubbles towards the ECCS suction strainer. So the axial and radial liquid velocity need to be scaled, respectively. Since the scalings for liquid velocity inside the SP are two-dimensional based on the axisymmetry assumption, the scaling approach for the axial liquid velocity is different from that for the radial liquid velocity. Figure 2.1 shows the schematic of the water column after vent clearing. It is assumed that a cylindrical water column inside downcomer is ejected when the inlet gas velocity is supplied. The axial liquid velocity is scaled by using the same approach used for the scaling of inlet velocity. So the axial liquid velocity is scaled by the length ratio as

$$v_{fz,R} = L_R \quad (2-12)$$

For the radial liquid velocity, it is assumed that the axial liquid volumetric flow rate is same as the radial liquid volumetric flow rate as

$$Q_f = v_{fz} \cdot \frac{\pi}{4} D^2 = v_{fr} \cdot \pi DL \quad (2-13)$$

Equation (2-13) is rewritten as

$$v_{fr} = v_{fz} \cdot \frac{D}{L} \quad (2-14)$$

Thus, the radial liquid velocity can be scaled as

$$v_{fr,R} = v_{fz,R} \cdot \frac{D_R}{L_R} = L_R \cdot \frac{D_R}{L_R} = D_R \quad (2-15)$$

Equation (2-15) indicates that the radial liquid velocity is scaled by the diameter ratio.

Table 2.1 Comparison between MARK-I and PUMA-E

Parameters	MARK I	PUMA-E
Power	3,300 MWth	630 kW (Maximum)
DW - Free Volume	4,142 m <sup>3</sup>	12.68 m <sup>3</sup>
Wetwell - Water Volume	2,453.7 m <sup>3</sup> (34.08 m <sup>3</sup> per downcomer)	8.05 m <sup>3</sup>
- Gas Space Volume	3,114.8 m <sup>3</sup>	9.38 m <sup>3</sup>
- Water Level	3.76 m	1.60 m
Vents - Orientation	Vertical	Horizontal
- Diameter of Downcomer	0.6 m	0.36 m
- Submerged Depth	1.32 m	0.43 m
- Number of Downcomers	72	1
Maximum Flow Rate per Downcomer	44.7 kg/s of steam*	0.5 kg/s of steam** (during blowdown)

\* based on data from NRC [5] \*\* based on the RELAP5 calculation

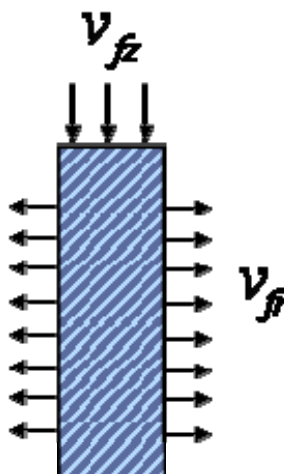


Figure 2.1 Schematic of Water Column after Vent Clearing.

## 2.2. Scaling for Facility Modification

The facility modification can be conducted using the geometry scaling ratio. To obtain the scaling ratio, the available water level (1.05 m) inside the SP of PUMA-E facility is measured. Since the geometry information for the MARK-I is known [5], the scaling ratio can be determined by those values.

Tables 2.2 and 2.3 show the dimensions and scaling ratios between the MARK-I and PUMA-E to perform the facility modification for the steady-state tests and transient tests, respectively. Both tests will be performed based on the 3 and 4 inch diameter downcomer sizes. As shown in Tables 2.2 and 2.3, the available water level in the SP of PUMA-E is 1.05 m and the length ratio is determined as  $1/3.58$ . By using the length ratio, the downcomer submergence depth in the SP of PUMA-E can be scaled as 0.37 m. The basic difference between the steady-state tests and transient tests is that the transient tests utilize the RPV and DW. However, it should be noted that although the DW free volume of PUMA-E shown in Table 2.1 is much larger than the required DW free volume shown in Table 2.3, modification of DW is not considered in this research.

Table 2.2 Scaling for Steady-State Tests

Parameter	MARK-I	PUMA-E (Modified)	Scaling Ratios	PUMA-E (Modified)	Scaling Ratios
		3-inch Sch40 Downcomer		4-inch Sch40 Downcomer	
Wetwell Water Level (m)	3.76	1.05	1/3.58 ( $L_R$ )	1.05	1/3.58 ( $L_R$ )
Downcomer Submergence Depth (m)	1.32	0.37	1/3.58 ( $L_R$ )	0.37	1/3.58 ( $L_R$ )
Downcomer Diameter (m)	0.60	0.078	1/7.7 ( $D_R$ )	0.102	1/5.9 ( $D_R$ )
Cross-Sectional Area of Downcomer (m <sup>2</sup> )	0.28	0.0048	1/59.3 ( $A_R$ )	0.0082	1/34.6 ( $A_R$ )
Air Mass Flow Rate at Downcomer (kg/s)	17.1*	0.081	1/212.4 ( $\dot{m}_R$ )	0.081	1/123.88 ( $\dot{m}_R$ )

\* based on data from NRC [5]

Table 2.3 Scaling for Transient Tests

Parameter	MARK-I	PUMA-E (Modified)	Scaling Ratios	PUMA-E (Modified)	Scaling Ratios
		3-inch Sch40 Downcomer		4-inch Sch40 Downcomer	
Wetwell Water Level (m)	3.76	1.05	1/3.58 ( $L_R$ )	1.05	1/3.58 ( $L_R$ )
Downcomer Submergence Depth (m)	1.32	0.37	1/3.58 ( $L_R$ )	0.37	1/3.58 ( $L_R$ )
Downcomer Diameter (m)	0.60	0.078	1/7.7 ( $D_R$ )	0.102	1/5.9 ( $D_R$ )
Cross-Sectional Area of Downcomer (m <sup>2</sup> )	0.28	0.0048	1/59.3 ( $A_R$ )	0.0082	1/34.60 ( $A_R$ )
Drywell Free Volume per Downcomer (m <sup>3</sup> )	57.53	0.27	1/212.4 ( $V_R$ )	0.47	1/123.88 ( $V_R$ )
Steam Mass Flow Rate at Downcomer (kg/s)	44.7	0.21	1/212.4 ( $\dot{m}_R$ )	0.36	1/123.88 ( $\dot{m}_R$ )

### 2.3. Demonstration of Scaling Approach

The scaling approach used in this research is preliminarily demonstrated by using Computational Fluid Dynamics (CFD). The purpose of CFD simulation is to confirm whether the venting phenomena which occur in the MARK-I can be reproduced in PUMA-E facility based on the current scaling approach.

The CFD simulation is performed to see the venting phenomena inside the SP of the MARK-I and PUMA-E. Figure 2.2 shows top and side views for the SP of the MARK-I and PUMA-E geometries used for the CFD simulation. The SP geometry of PUMA-E is created based on the length ratio (1/3.58) for the axial direction and diameter ratio (3 inch, 1/7.7) for the radial direction. The geometry of the SP is assumed to be a cylindrical shape. A quarter section of it is considered in the simulation. ANSYS CFX is used for the CFD solver. The details of the CFD simulation are summarized in Table 2.5. Table 2.4 shows the inlet boundary conditions for the MARK-I and PUMA-E, which was suggested by NRC [6]. The inlet boundary condition for DBA highlighted on Table 2.4 is applied to the MARK-I and value scaled by length ratio (1/3.58) is applied to PUMA-E. It is noted that since the CFD results with 2 inch downcomer showed relatively large viscous effect, 2 inch downcomer test will be changed to 4 inch downcomer in actual experiments. Figures 2.3 and 2.4 show the inlet gas velocities with time applied to the MARK-I and PUMA-E. It is assumed in Figures 2.3 and 2.4 that the initial 2 seconds represents the valve stroke time to simulate the pressure buildup. During the initial 2 seconds, the inlet gas velocity increases linearly and finally reaches the maximum condition.

Figure 2.5 shows the void distribution inside SP before the vent clearing time for the MARK-I and PUMA-E. When the inlet boundary condition is set up, the water column inside downcomer starts to accelerate and eject. The vent clearing time is 0.34 second for both the MARK-I and PUMA-E. As shown in Figure 2.6, The air starts to be vented into the SP through the downcomer after the water column inside downcomer is completely vented. Initially the air flow penetrates into the water inside the SP, but the air inertia is relatively small compared to the water inertia. Thus the air cannot penetrate

further into the water. Finally a big bubble is formed around downcomer exit. It can be seen that these phenomena occur both in the MARK-I and PUMA-E. However, the timing of big bubble formation around downcomer exit in the PUMA-E is slightly earlier than that in the MARK-I. The reason is not clear, but the real phenomena will be investigated through experiments. After the big bubble is formed around downcomer exit, the bubble plume starts to move upward due to the buoyancy force as shown in Figure 2.6. Then, most of air flow directly move upward even though the inlet air velocity increases continuously with time as shown in Figures 2.7 and 2.8. It is noted that the venting phenomena shown in Figures 2.5 through 2.8 occurs within 2 seconds from the initial air boundary flow. Although there are slight differences between the MARK-I and PUMA-E, it may be said that most of the venting phenomena shown in MARK-I is reproduced in ideally scaled PUMA-E based on the CFD simulation results.

On the other hand, the axial and radial liquid velocity distributions inside SP are also important parameters. Figure 2.9 shows the axial liquid velocity distributions inside SP of MARK-I and PUMA-E before the vent clearing time ( $t = 0.5\tau_{vc}$ ). At this time, the venting phenomena inside SP is totally single phase flow. The axial liquid velocity distribution of the MARK-I is globally similar to that of the PUMA-E. Figure 2.10 indicates the radial liquid velocity distribution inside SP of MARK-I and PUMA-E before the vent clearing time ( $t = 0.5\tau_{vc}$ ). It is seen that the radial liquid velocity distribution of the MARK-I is also globally similar to that of the PUMA-E. The left, middle and right graphes shown in Figure 2.11 represent the local axial liquid velocity distribution, local radial liquid velocity distribution in lower part of SP and local radial liquid velocity distribution in upper part of SP, respectively. The results of PUMA-E is already scaled up to compare with those of MARK-I as

$$v_{fz,m} / L_R \quad (2-16)$$

and

$$v_{fr,m} / D_R \quad (2-17)$$

It can be seen that local axial and radial liquid velocity profiles of the MARK-I are similar to those of the PUMA-E before the vent clearing time. Figures 2.12, 2.13 and 2.14

show the corresponding results at the vent clearing time ( $t = 1.0\tau_{vc}$ ). It can be seen that the global/local axial and radial liquid velocity distributions of the MARK-I are similar to those of the PUMA-E. Figures 2.15 through 2.17 indicate the results after vent clearing time ( $t = 1.5\tau_{vc}$ ). The global/local axial and radial liquid velocity distributions of the phenomena in the MARK-I are somewhat different from those of the PUMA-E due to the slight difference of the timing of big bubble formation around the downcomer exit. These difference are still seen in Figures 2.18 through 2.20, which show the results after the vent clearing time ( $t = 2.5\tau_{vc}$ ). However it can be seen in Figures 2.21 through 2.23 ( $t = 4.0\tau_{vc}$ ) that the global/local axial and radial liquid velocity distributions recover the similarity between the MARK-I and PUMA-E after the bubble plume formed around downcomer exit moves upward, and the similarity continues as shown in Figures 2.24 through 2.26 ( $t = 6.0\tau_{vc}$ ).

Based on the preliminary CFD simulation results for the venting phenomena of the SP between the MARK-I and ideally scaled PUMA-E, the venting phenomena that occurs in the MARK-I can be reproduced in the ideally scaled PUMA-E. It may be said that the current scaling approach described in section 2.1 is reasonable.

Table 2.4 Inlet Boundary Conditions Suggested by NRC [6]

(@113.4 KPa & 65.5degC, 1.16 kg/m<sup>3</sup>)

						2-inches Sch40 Downcomer (scaling factor 1/467.6)		3-inches Sch40 Downcomer (scaling factor 1/212.4)	
			Volumetric Flow (m <sup>3</sup> /s)	Mass Flow Rate (kg/s)	Velocity (m/s)	Mass Flow Rate (kg/s)	Velocity (m/s)	Mass Flow Rate (kg/s)	Velocity (m/s)
Proposed by Purdue			10.9	12.6	38.4	0.026	10.33	0.059	10.70
Suggested by NRC	Medium	Category 2	0.5	0.6	1.7	0.001	0.47	0.003	0.48
		Category 3	1.6	1.9	5.8	0.004	1.56	0.009	1.61
	Large	Category 4	8.2	9.5	28.9	0.020	7.78	0.045	8.06
		DBA	14.8	17.1	52.3	0.036	14.05	0.081	14.56

Table 2.5 Details of CFD Simulation

	Models	Remarks
Simulation Type	Transient	
Governing Equation	Two-fluid model	Gas phase: air Liquid phase: water
Turbulence Model	Standard $k - \varepsilon$	
Bubble Diameter	5 mm	
Momentum Transfer Model	Drag force	Ishii and Zuber's model
Mesh Type	Unstructured tetrahedral	
Inlet Boundary	Velocity	Profile with time
Outlet Boundary	Pressure	
Wall Boundary	Gas phase : free slip Liquid phase: no slip	

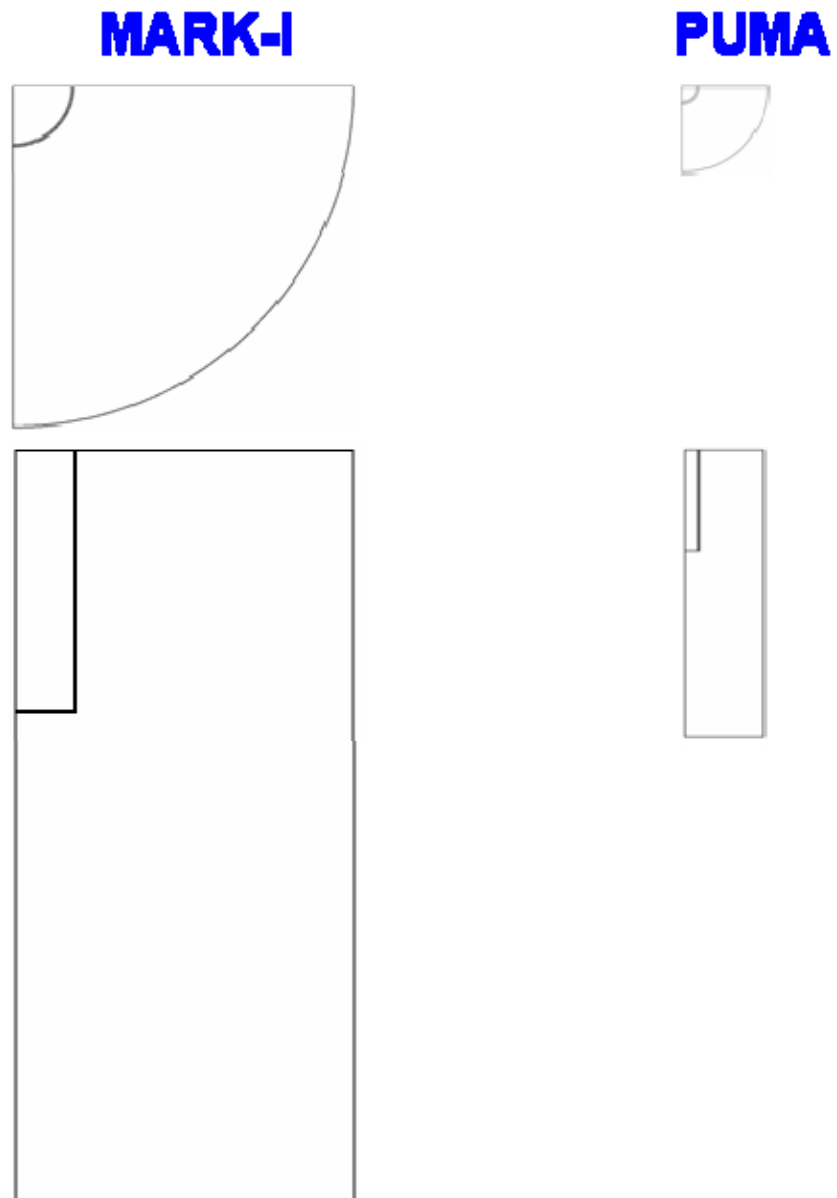


Figure 2.2 SP Geometries for MARK-I and PUMA-E to Perform CFD Simulation.

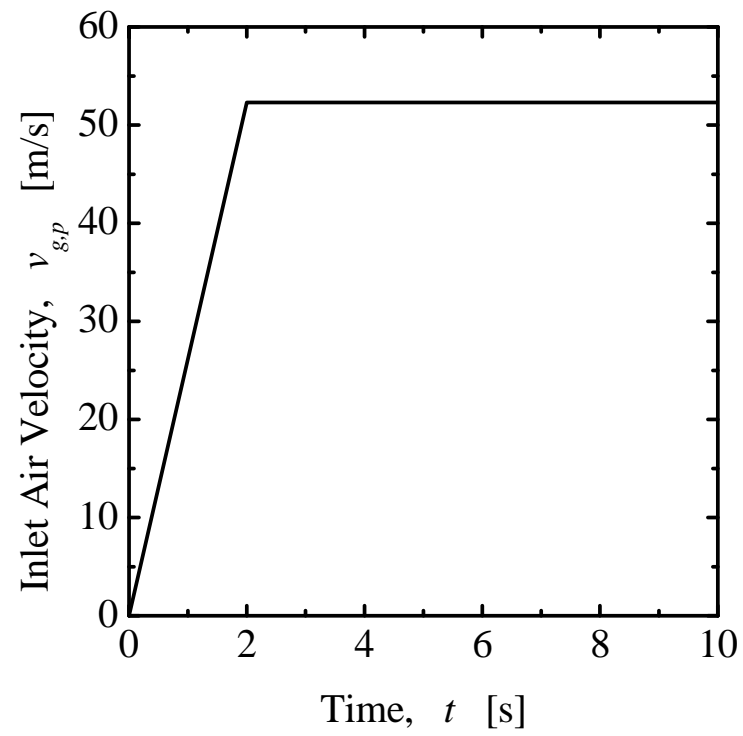


Figure 2.3 Inlet Boundary Condition Applied to MARK-I

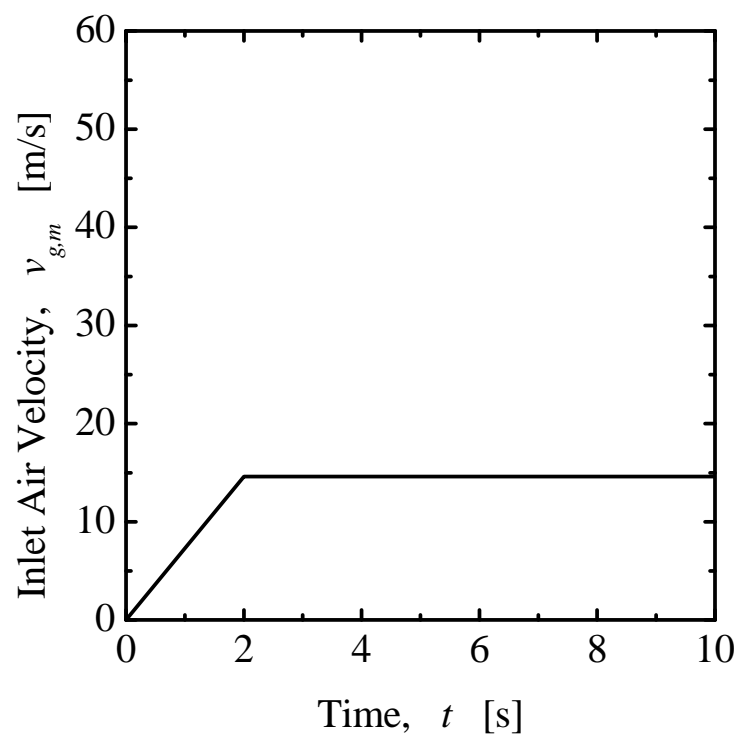


Figure 2.4 Inlet Boundary Condition Applied to PUMA-E.

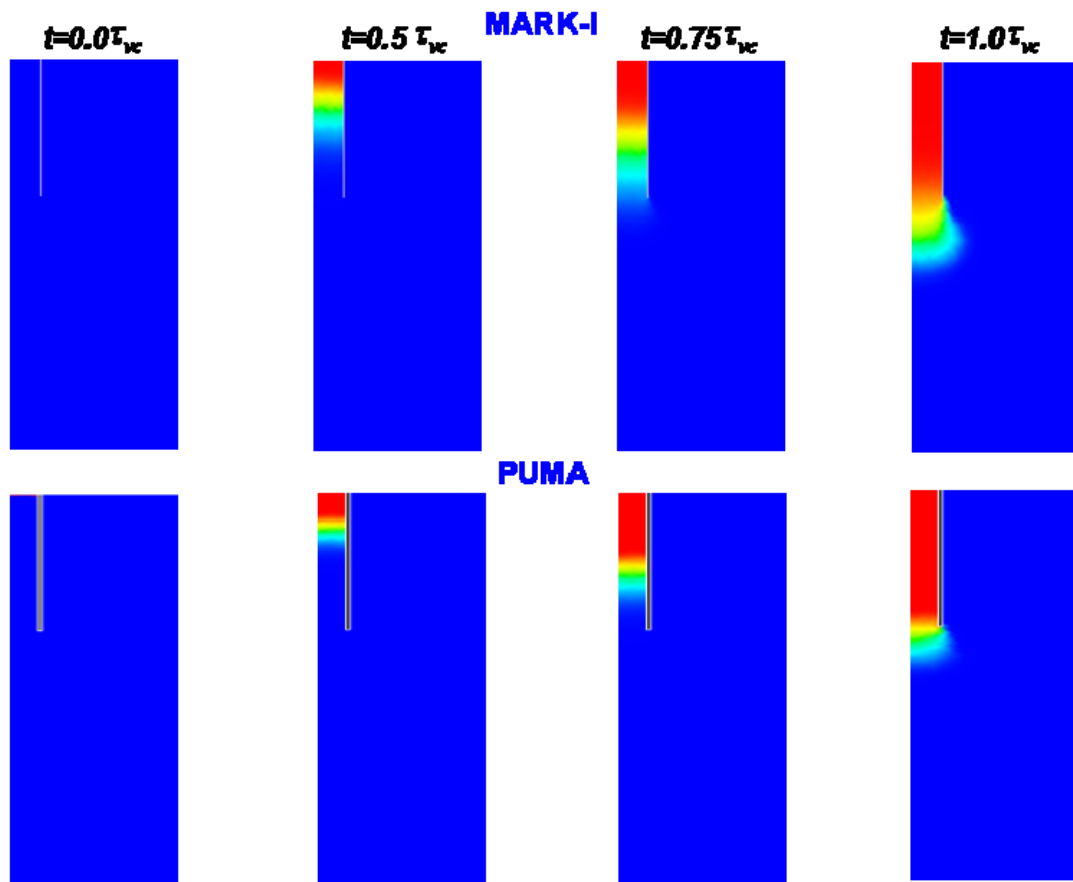


Figure 2.5 Void Distribution with Time (MARK-I and PUMA-E 3'' Downcomer,  $\tau_{vc} = 0.34$  second,  $0.0\tau_{vc} \leq t \leq 1.0\tau_{vc}$ ).

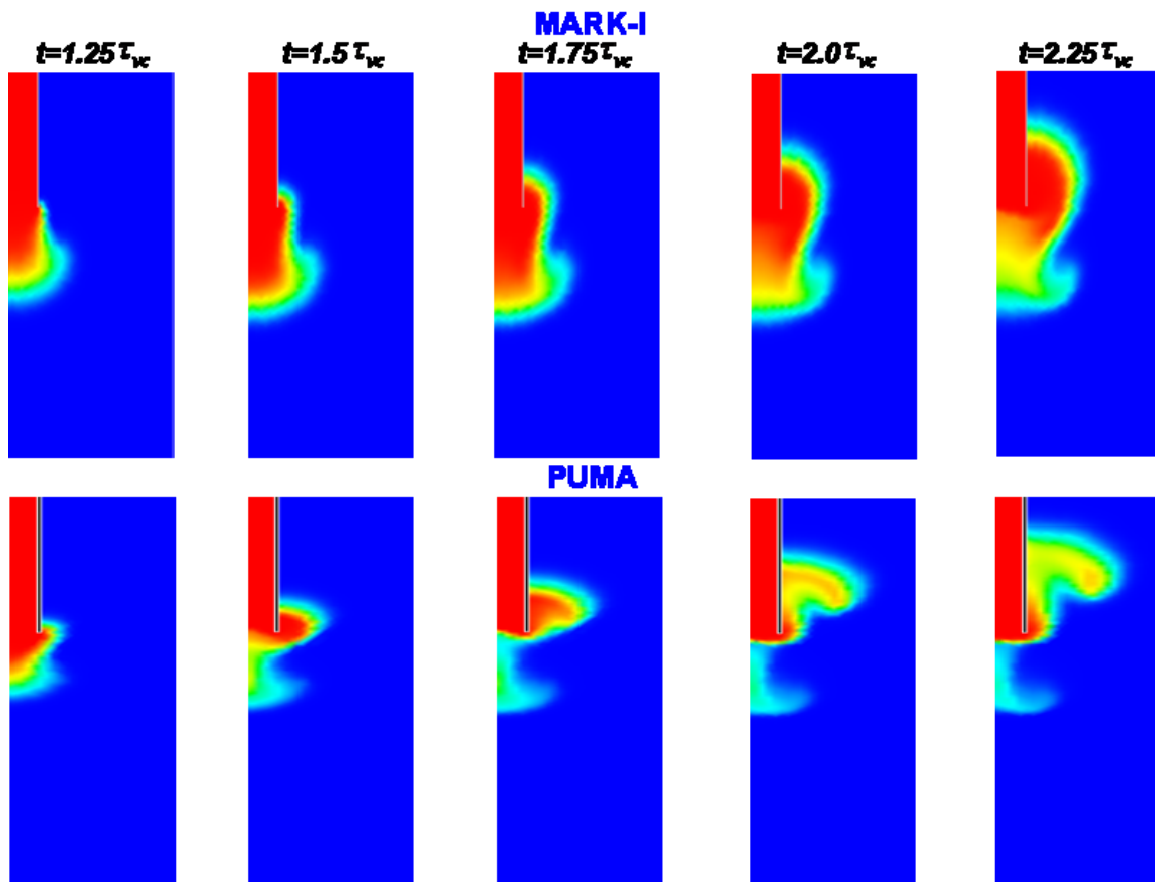


Figure 2.6 Void Distribution with Time (MARK-I and PUMA-E 3'' Downcomer,  $\tau_{vc}=0.34$  second,  $1.25\tau_{vc} \leq t \leq 2.25\tau_{vc}$  ).

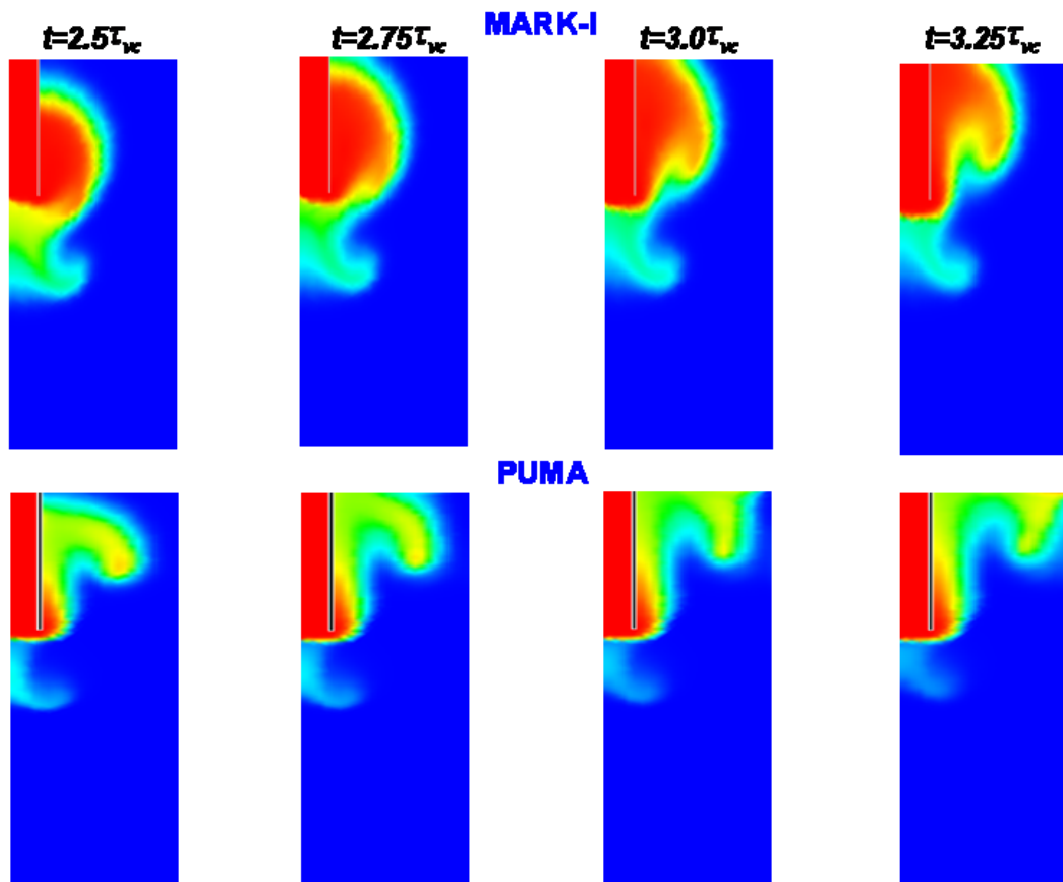


Figure 2.7 Void Distribution with Time (MARK-I and PUMA-E 3'' Downcomer,  $\tau_{vc}=0.34$  second,  $2.5\tau_{vc} \leq t \leq 3.25\tau_{vc}$ ).

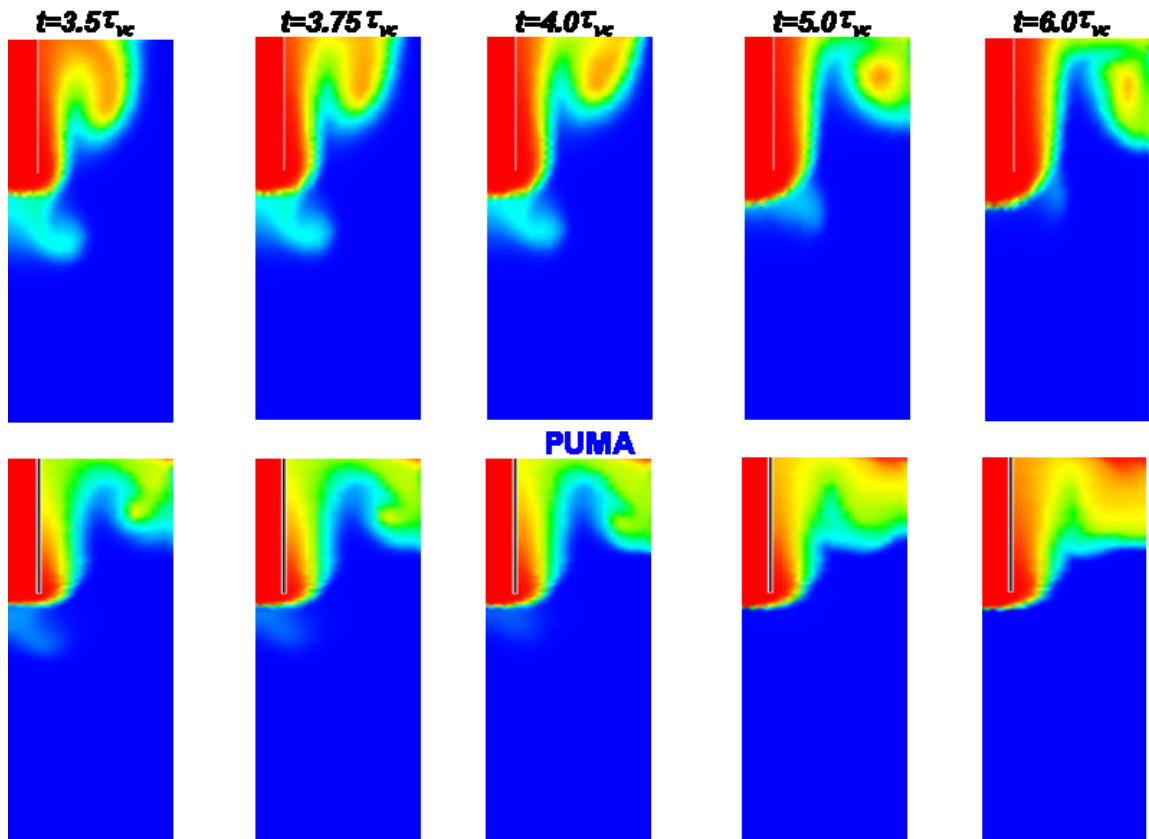


Figure 2.8 Void Distribution with Time (MARK-I and PUMA-E 3'' Downcomer,  
 $\tau_{vc} = 0.34$  second,  $3.5\tau_{vc} \leq t \leq 6.0\tau_{vc}$ ).

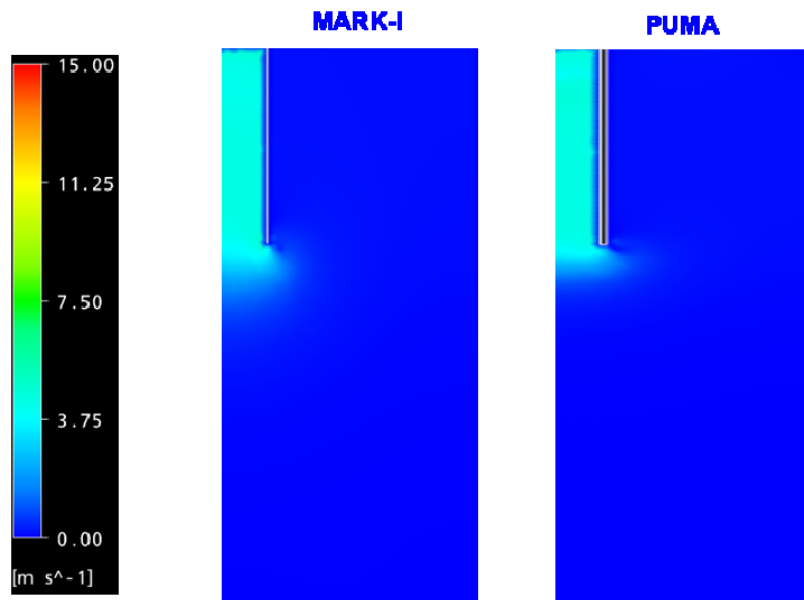


Figure 2.9 Axial Liquid Velocity Distribution (MARK-I and PUMA-E 3'' Downcomer,  $\tau_{vc}=0.34$  second,  $t = 0.5\tau_{vc}$ ).

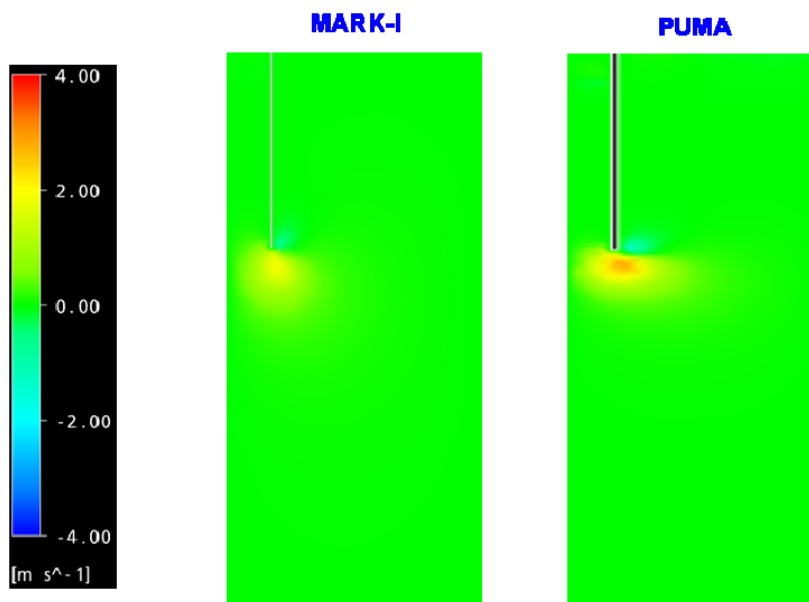


Figure 2.10 Radial Liquid Velocity Distribution (MARK-I and PUMA-E 3'' Downcomer,  $\tau_{vc}=0.34$  second,  $t = 0.5\tau_{vc}$ ).

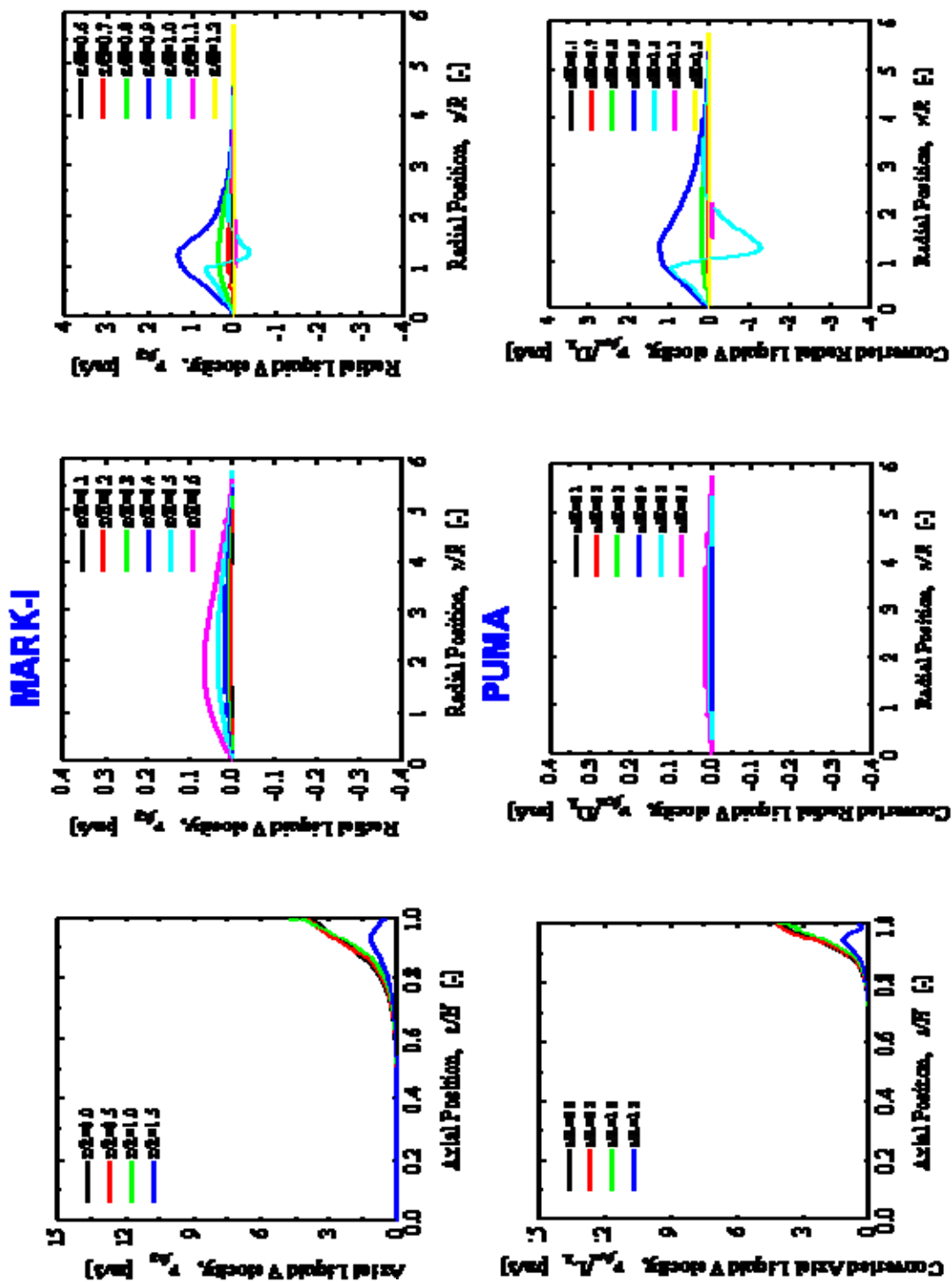


Figure 2.11 Local Axial and Radial Liquid Velocity Distributions (MARK-I and PUMA-E 3" Downcomer,  $\tau_{vc}=0.34$  second,  $t = 0.5\tau_{vc}$ ).

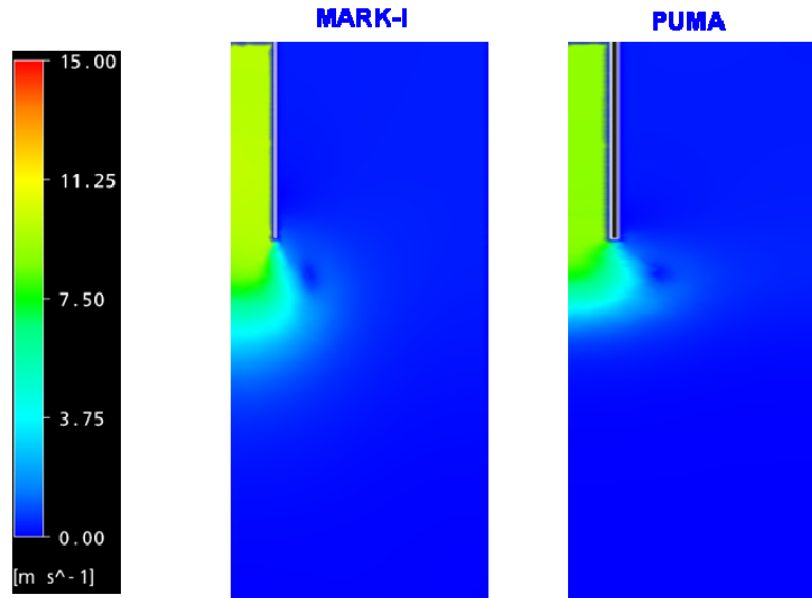


Figure 2.12 Axial Liquid Velocity Distribution (MARK-I and PUMA-E 3'' Downcomer,  $\tau_{vc}=0.34$  second,  $t = 1.0\tau_{vc}$ ).

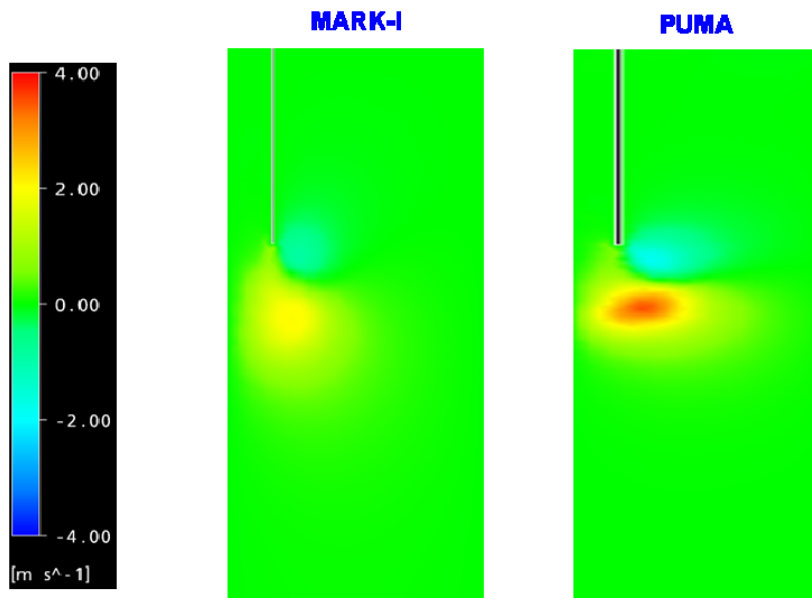


Figure 2.13 Radial Liquid Velocity Distribution (MARK-I and PUMA-E 3'' Downcomer,  $\tau_{vc}=0.34$  second,  $t = 1.0\tau_{vc}$ ).

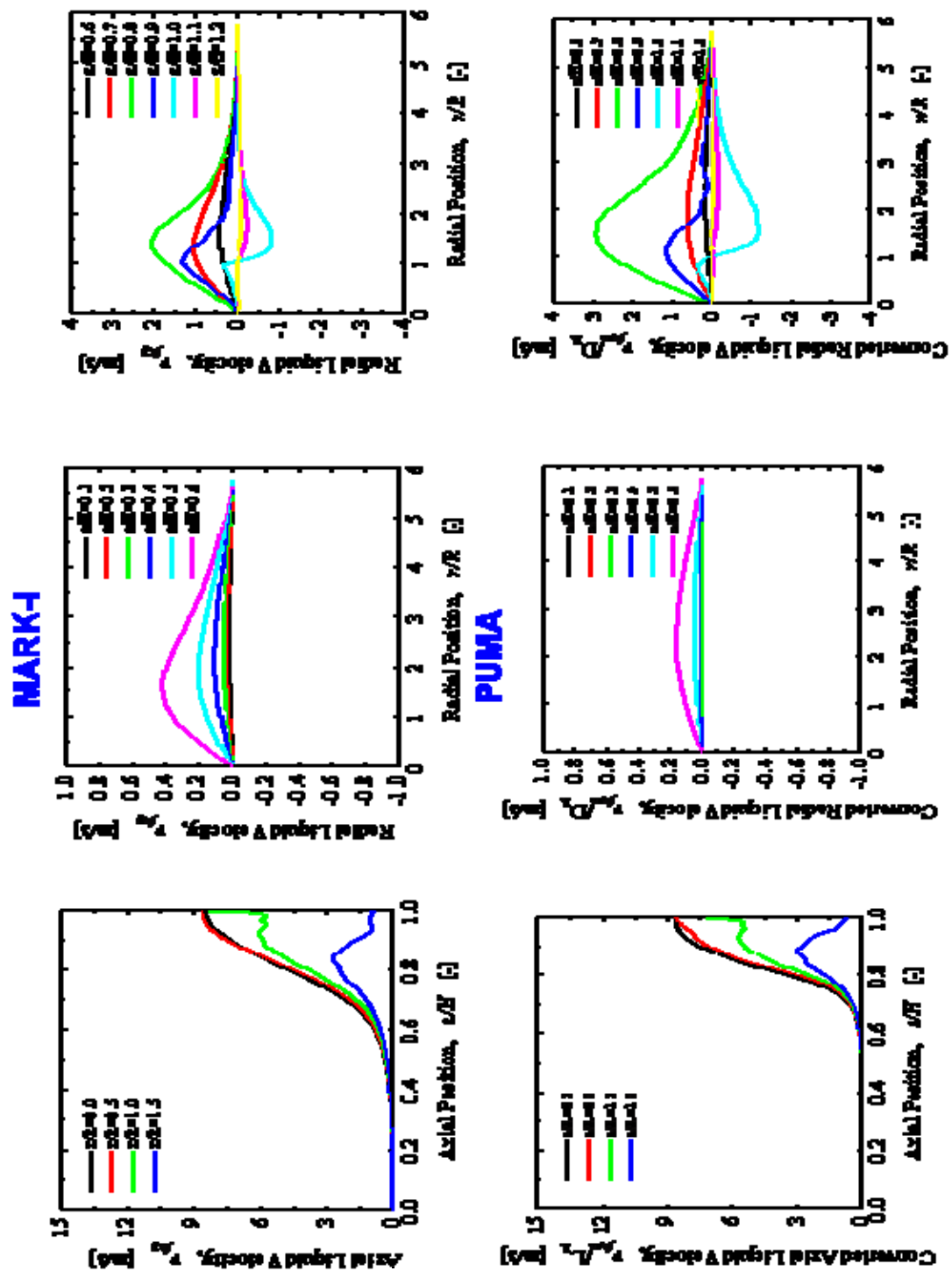


Figure 2.14 Local Axial and Radial Liquid Velocity Distributions (MARK-I and PUMA-E 3" Downcomer,  $\tau_{vc}=0.34$  second,  $t=1.0\tau_{vc}$ ).

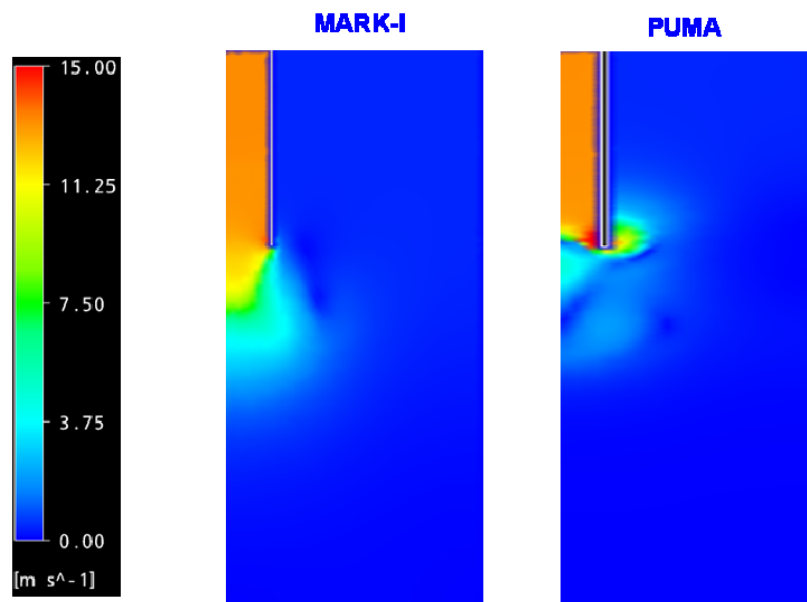


Figure 2.15 Axial Liquid Velocity Distribution (MARK-I and PUMA-E 3'' Downcomer,  $\tau_{vc}=0.34$  second,  $t = 1.5\tau_{vc}$ ).

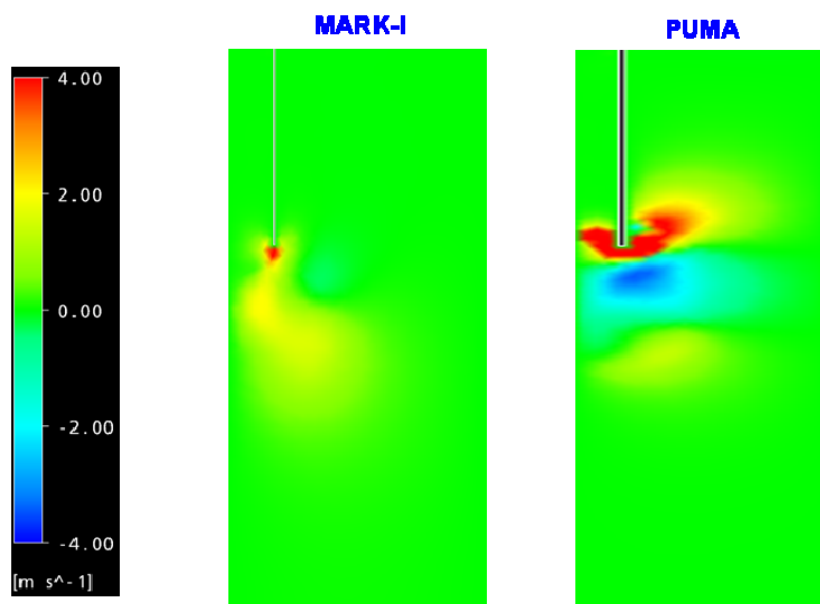


Figure 2.16 Radial Liquid Velocity Distribution (MARK-I and PUMA-E 3'' Downcomer,  $\tau_{vc}=0.34$  second,  $t = 1.5\tau_{vc}$ ).

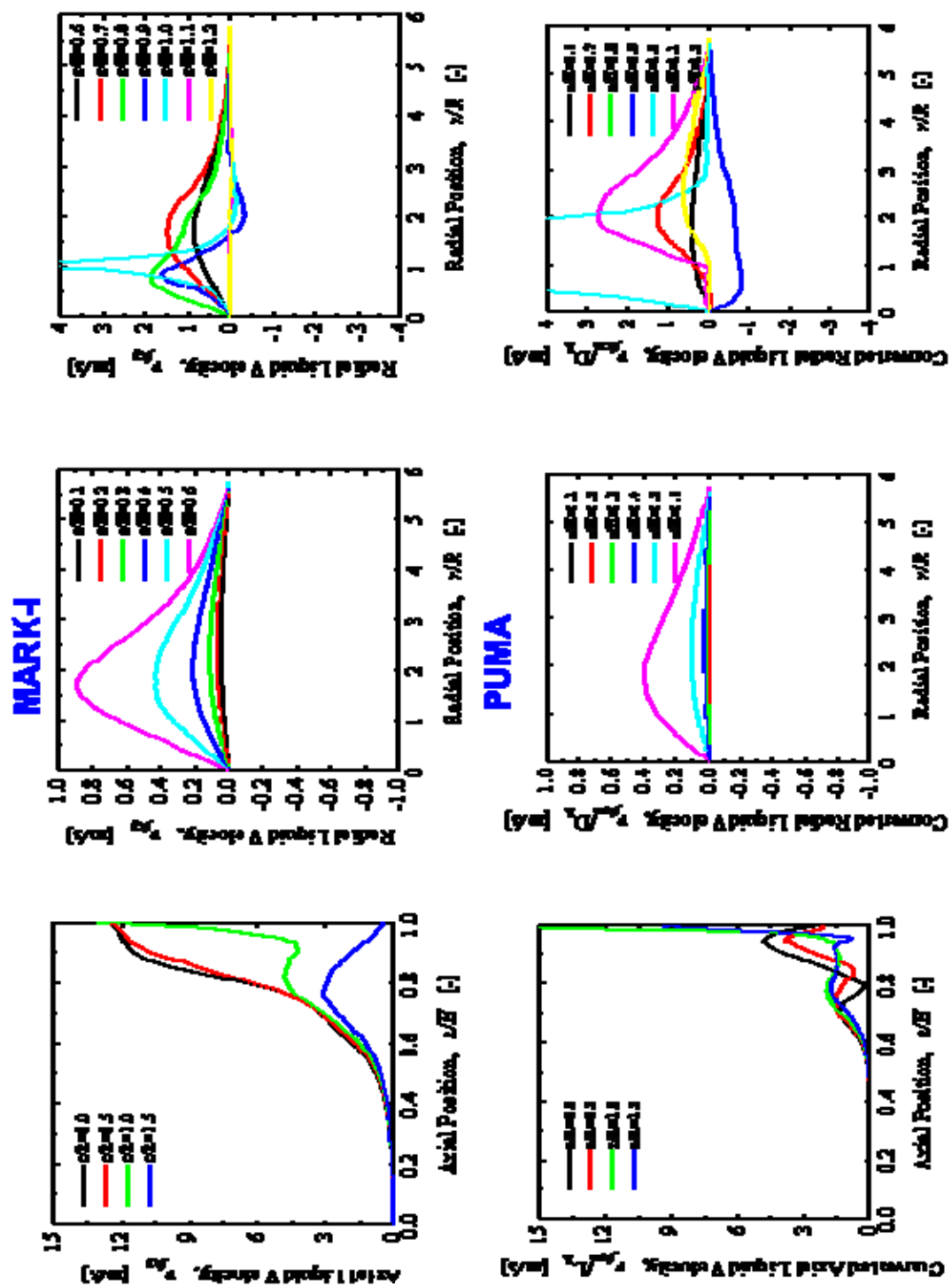


Figure 2.17 Local Axial and Radial Liquid Velocity Distributions (MARK-I and PUMA-E 3" Downcomer,  $\tau_{vc}=0.34$  second,  $t=1.5\tau_{vc}$ ).

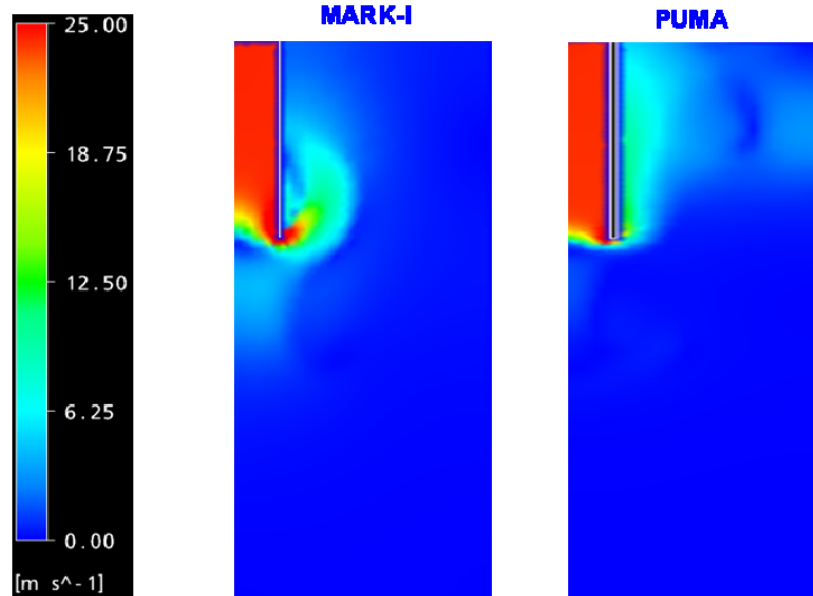


Figure 2.18 Axial Liquid Velocity Distribution (MARK-I and PUMA-E 3'' Downcomer,  
 $\tau_{vc}=0.34$  second,  $t = 2.5\tau_{vc}$ )

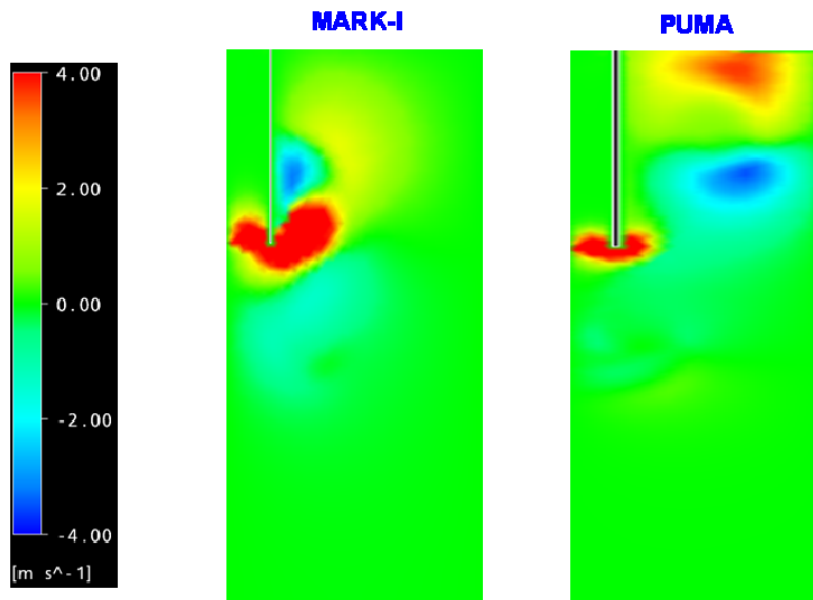


Figure 2.19 Radial Liquid Velocity Distribution (MARK-I and PUMA-E 3'' Downcomer,  
 $\tau_{vc}=0.34$  second,  $t = 2.5\tau_{vc}$ ).

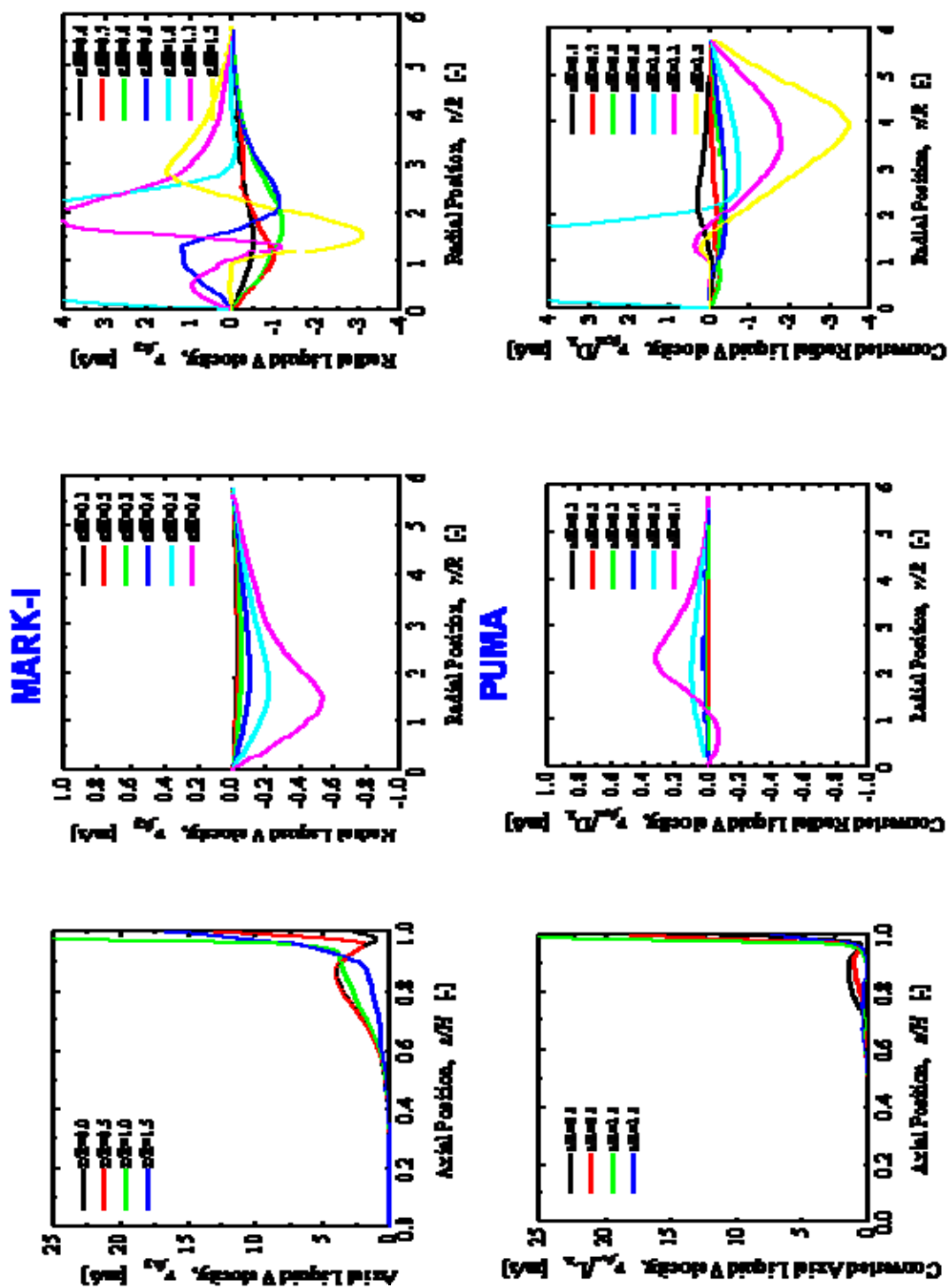


Figure 2.20 Local Axial and Radial Liquid Velocity Distributions (MARK-I and PUMA-

E 3" Downcomer,  $\tau_{vc}=0.34$  second,  $t = 2.5\tau_{vc}$ ).

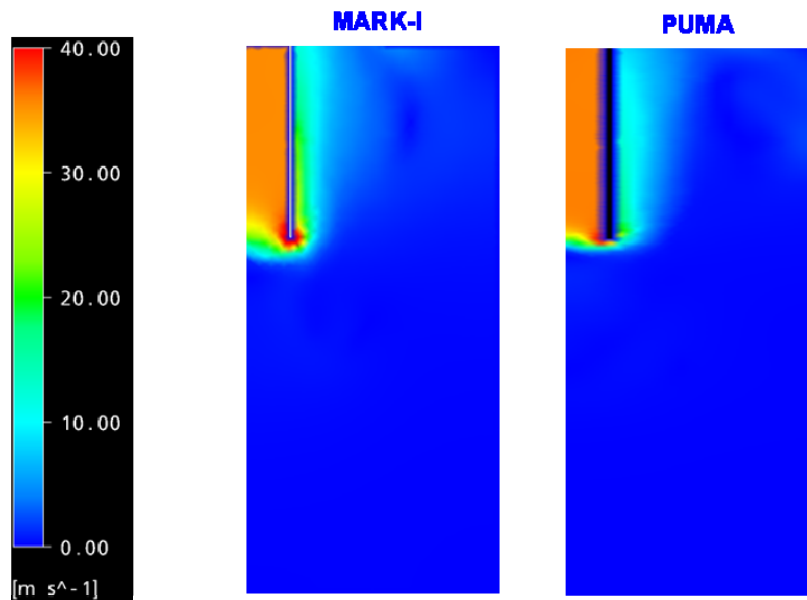


Figure 2.21 Axial Liquid Velocity Distribution (MARK-I and PUMA-E 3'' Downcomer,  $\tau_{vc}=0.34$  second,  $t = 4.0\tau_{vc}$ ).

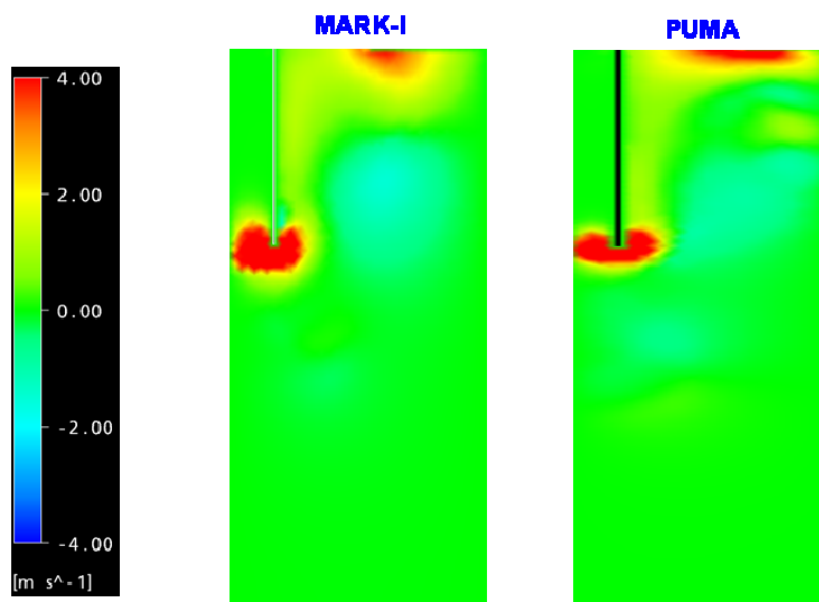


Figure 2.22 Radial Liquid Velocity Distribution (MARK-I and PUMA-E 3'' Downcomer,  $\tau_{vc}=0.34$  second,  $t = 4.0\tau_{vc}$ ).

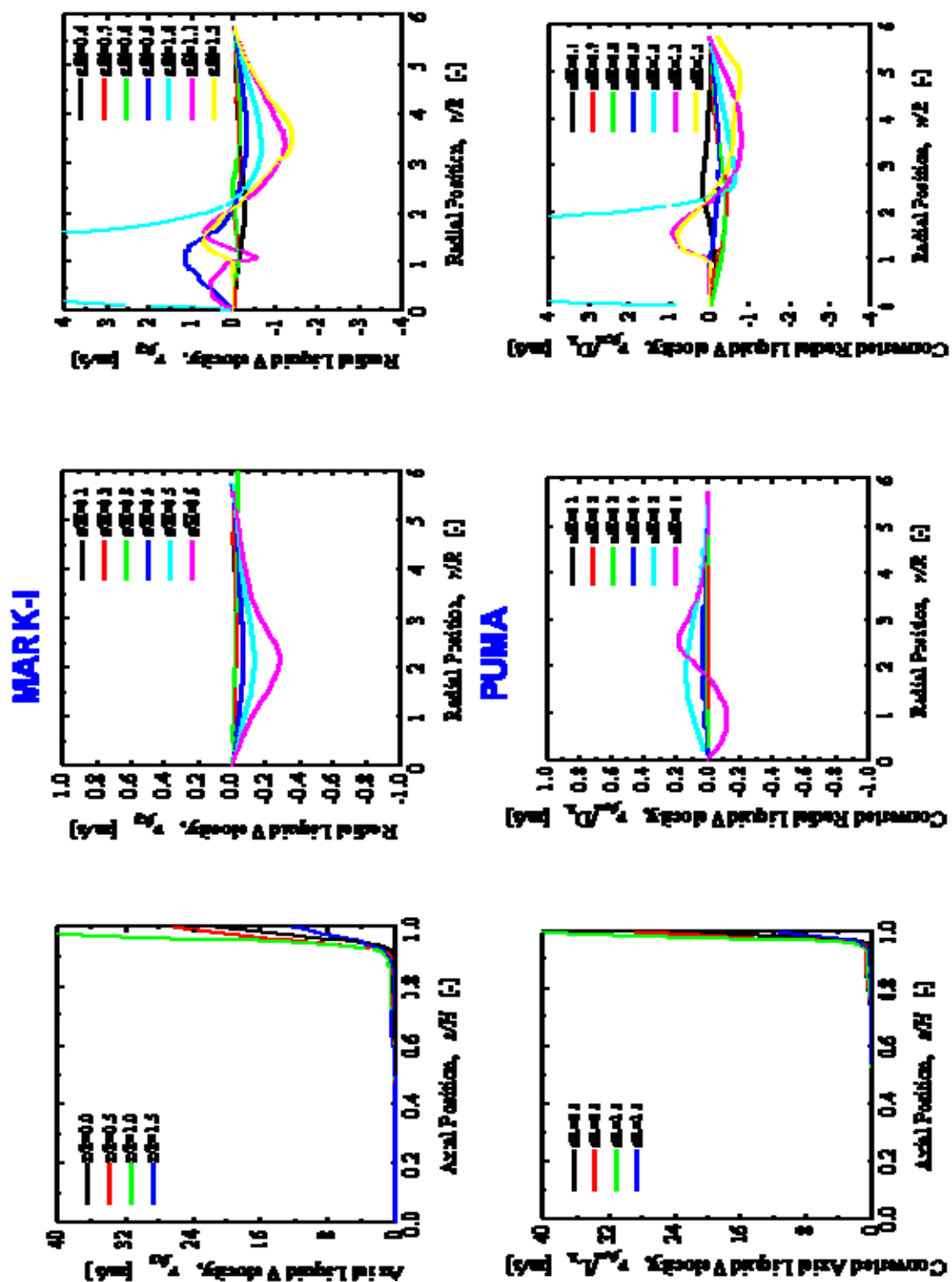


Figure 2.23 Local Axial and Radial Liquid Velocity Distributions (MARK-I and PUMA-E 3" Downcomer,  $\tau_{vc}=0.34$  second,  $t = 4.0\tau_{vc}$ ).

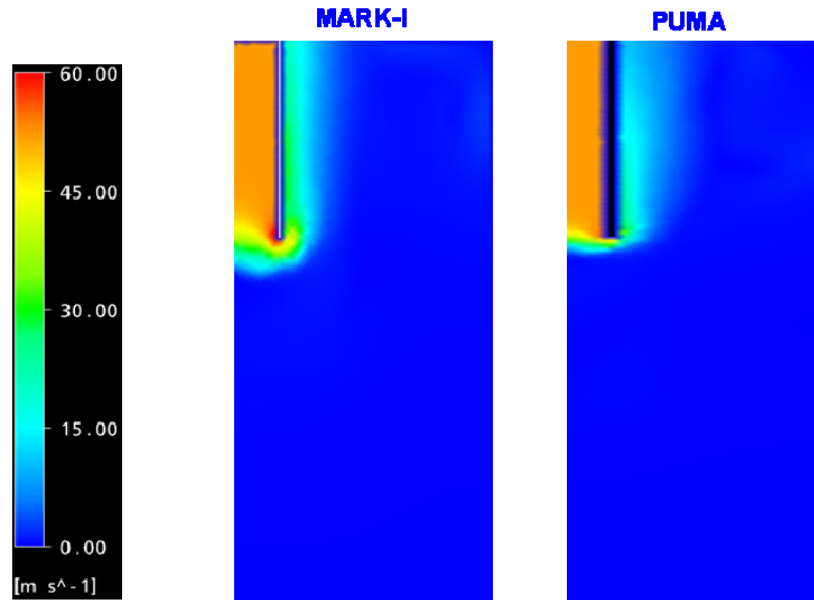


Figure 2.24 Axial Liquid Velocity Distribution (MARK-I and PUMA-E 3'' Downcomer,  $\tau_{vc}=0.34$  second,  $t = 6.0\tau_{vc}$ ).

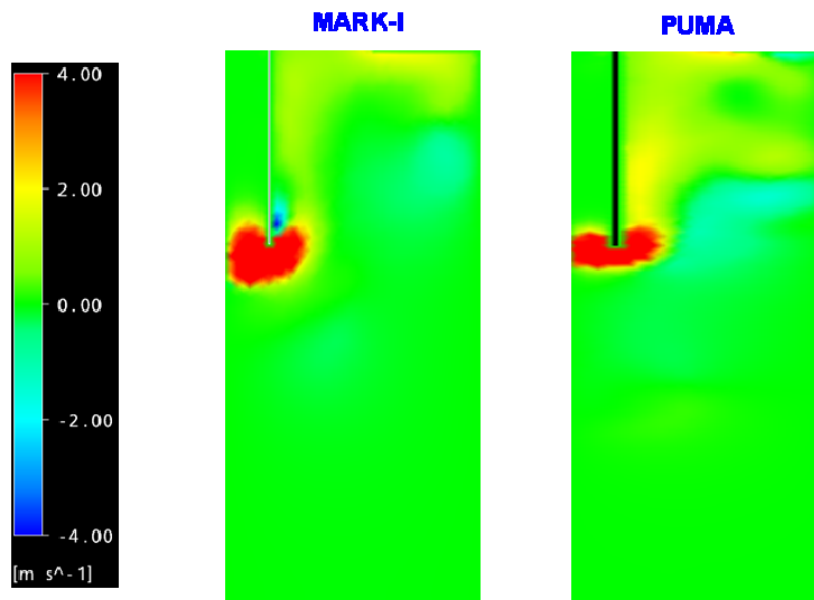


Figure 2.25 Radial Liquid Velocity Distribution (MARK-I and PUMA-E 3'' Downcomer,  $\tau_{vc}=0.34$  second,  $t = 6.0\tau_{vc}$ ).

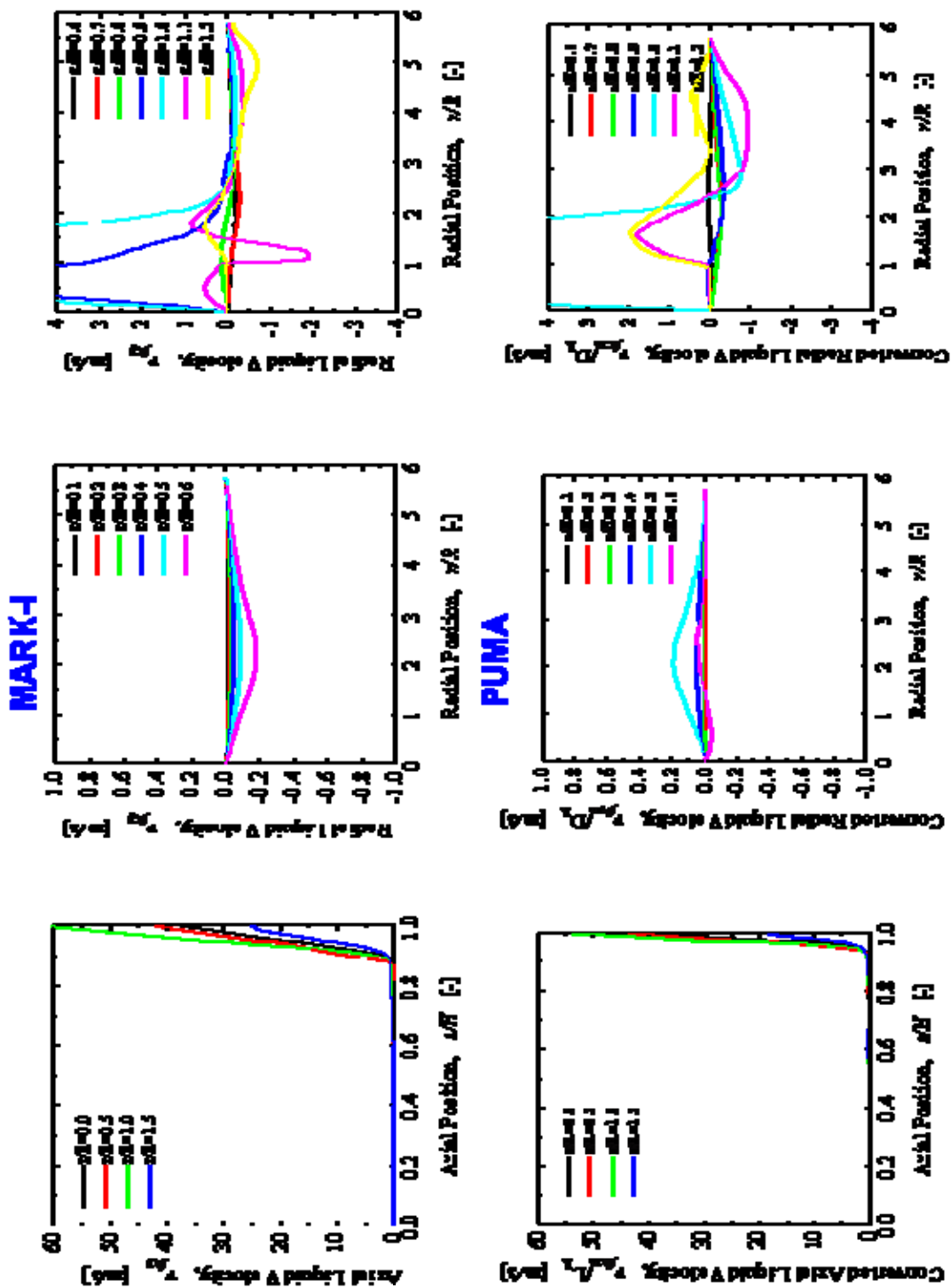


Figure 2.26 Local Axial and Radial Liquid Velocity Distributions (MARK-I and PUMA-E 3" Downcomer,  $\tau_{vc}=0.34$  second,  $t = 6.0\tau_{vc}$ ).

## CHAPTER 3. FACILITY MODIFICATION

In order to use the PUMA-E facility to investigate the void distribution and fluid dynamics of the BWR SP during the blowdown, facility modification and installation of instrumentation are necessary for both the steady-state and transient tests.

### 3.1. Facility Modification for Steady-State Tests

The air injection system will be constructed in the PUMA-E facility to provide the required air flow rate for the downcomer pipe section in the steady-state experiments. The 3-inch or 4-inch downcomer pipe will be installed in the SP of PUMA-E facility to simulate downcomer in suppression chamber in the MARK-I containment. The dimensions of the downcomer pipe and submerged depth of pipe in the SP will be determined by the scaling results as shown in Tables 2.2 and 2.3.

#### 3.1.1. Air Injection System for Steady-State Tests

Figure 3.1 shows the schematics of the test facility for steady-state tests. In the PUMA-E facility, the Safety Relief Valve (SRV) line is branched from the Main Steam Line (MSL) and connects the SP. Therefore, the new air injection line will be installed and merged into the exiting SRV line outside the SP to supply air flow to the downcomer pipe section. Valve (V-AL-08) will be used to isolate the flow from the PUMA-E RPV to the SP.

Generally, the required flow rate will be calibrated with a degree of the manual valve opening (V-AL-02) before the actual test. The pneumatic actuator valve (V-AL-03)

will be used to start the experiment by fully opening within a short period. The bypass line with 1/4-inch diameter and a valve (V-AL-04) branched from the 2-inch pipe line will be utilized to adjust the initial water level in the downcomer pipe inside SP before starting the experiment.

Near the location of pneumatic actuator valve, there are two branches of 2-inch and 3/4-inch pipe line with manual valves. The 2-inch pipe line will be used for the experiments with high flow rate condition while the 3/4-inch pipe line will be utilized for the experiments with relatively low flow rate condition. The reason for installation of the 3/4-inch pipe line is that the range of the vortex flow meter on 2-inch pipe line cannot cover the required low flow rate condition of the steady-state tests.

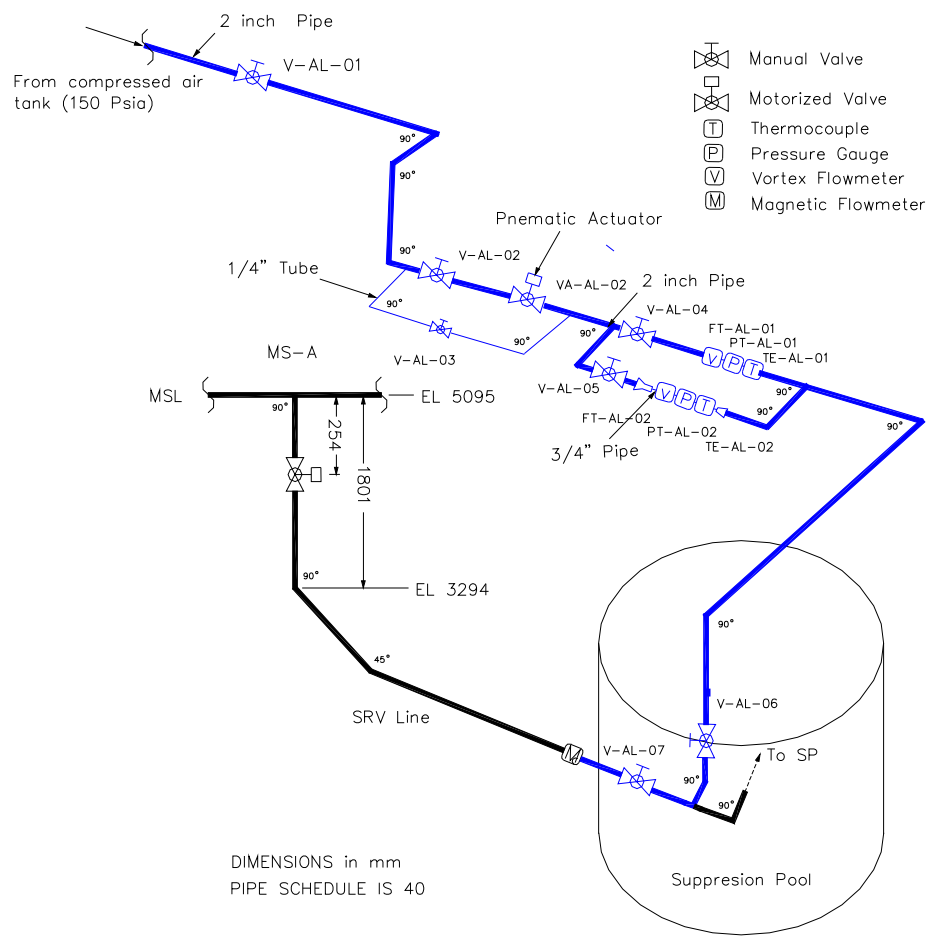


Figure 3.1 Experimental Facility for Steady-State Tests.

### 3.1.2. Downcomer Section for Steady-State Tests

Figures 3.2 and 3.3 show the side and top views of the SP with the modification of the SRV line, respectively. The downcomer pipe will be installed by modifying the SRV line inside the SP of PUMA-E. The existing SRV line with a 2-inch pipe can be replaced with 3-inch or 4-inch pipe for the test purpose.

The pipe lines are composed of two different materials, namely, stainless steel pipe and transparent lexan pipe. The transparent lexan pipe section will be extended from the around 20 cm above the SP water level and be submerged into water with the submergence depth of 37 cm. The transparent lexan pipe section can be used to measure the water column velocity in the downcomer by visualization of the water column-air interface location change using a high speed video camera. As a redundant measurement for the water column velocity based on the visual recording, 5 single-sensor conductivity probes will be mounted into the transparent pipe wall evenly to measure the water column velocity.

To measure the void distribution near the exit of the downcomer pipe, conductivity probes will be mounted in the supporting cage. Additionally, a 6-inch gas vent line will be installed on the available 4-inch pipe line at the top of the SP. Then, the gas vent line will be connected to atmosphere. The gas vent line will help to prevent over-pressurization of the SP during air injection and keep the pressure inside the SP at atmospheric pressure.

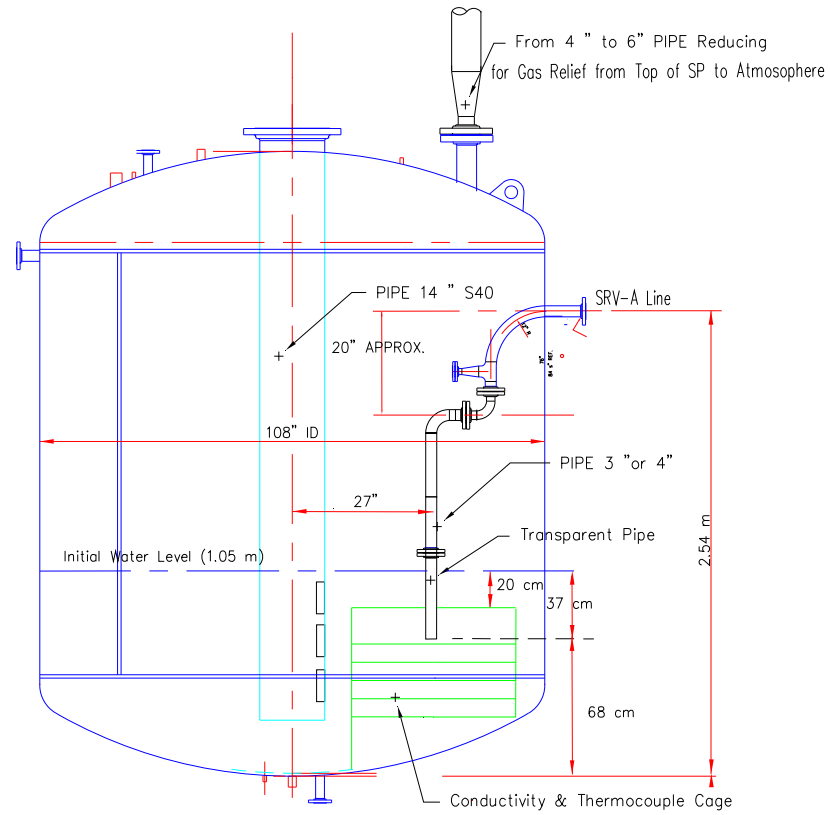


Figure 3.2 Side View of SP with Modification for Steady-State Tests.

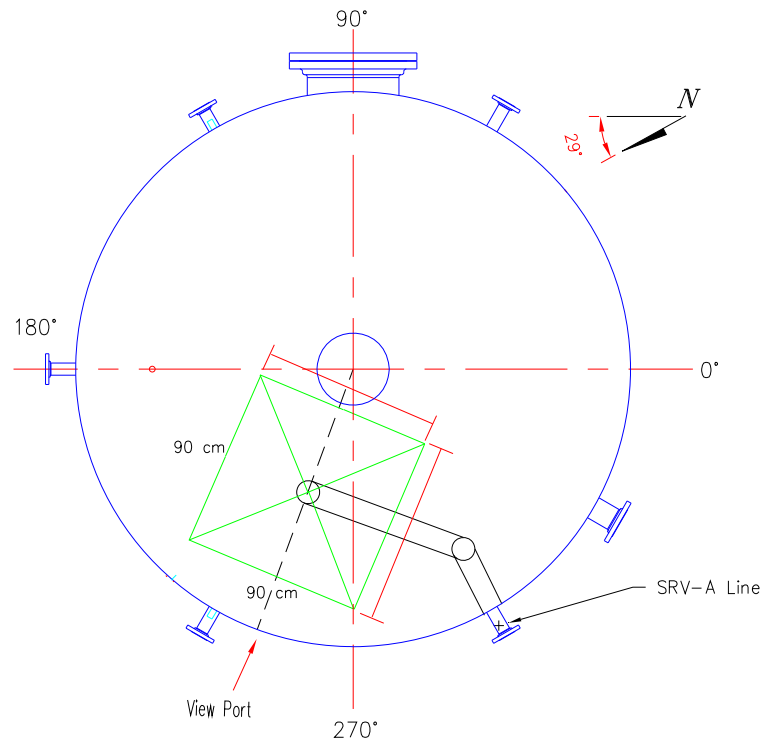


Figure 3.3 Top View of SP with Modification for Steady-State Tests.

### 3.2. Facility Modification for Transient Tests

To study the dynamics of DW to SP venting phenomena during the blowdown and void distribution in SP, the existing components such as the RPV, DW, vertical vent line, and SP in the PUMA-E facility will be utilized to perform the transient tests. Figure 3.4 represents the test facility for the transient tests.

A venting pipe needs to be installed on the existing vertical vent line as shown in Figure 3.5. A stainless steel pipe with 4-inch or 3-inch diameter will be mounted on a window of the vertical vent while the other window will be completely closed (In original PUMA-E vertical vent pipe, there are totally 9 windows). The stainless steel pipe will be connected to a 4-inch or 3-inch transparent lexan pipe before submerging into the water. Figure 3.6 shows the top view of the SP with the modification. A supporting cage for conductivity probes and thermocouples will be installed near the exit of the downcomer. The details of the supporting cage and probes design will be explained in section 4.1.1.

The single- and double-sensor conductivity probes will be used to measure the local void fraction, bubble size (or chord length) and interfacial velocity. Those probes will be mounted on the supporting cage at the designed positions. The facility will be also equipped with the thermocouples in the locations on the supporting cage. The gas sampling line for the oxygen analyzer will be installed inside the vertical vent pipe to measure air concentration during the test. The local instrumentations inside the SP and supporting cage will be shared for both the steady-state and transient tests. The details of each instrument will be explained in the Chapter 4.

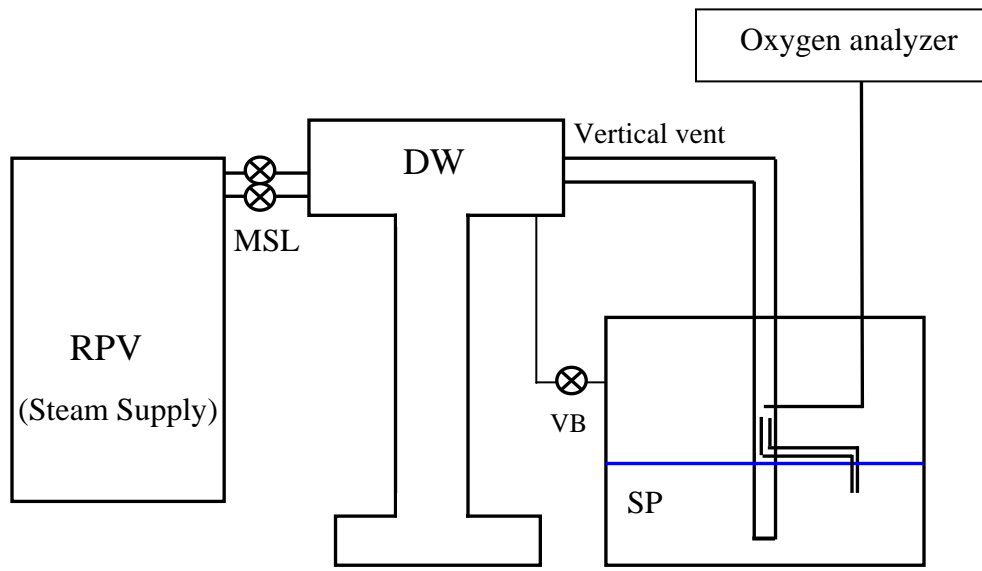


Figure 3.4 Experimental Facility for Transient Tests.

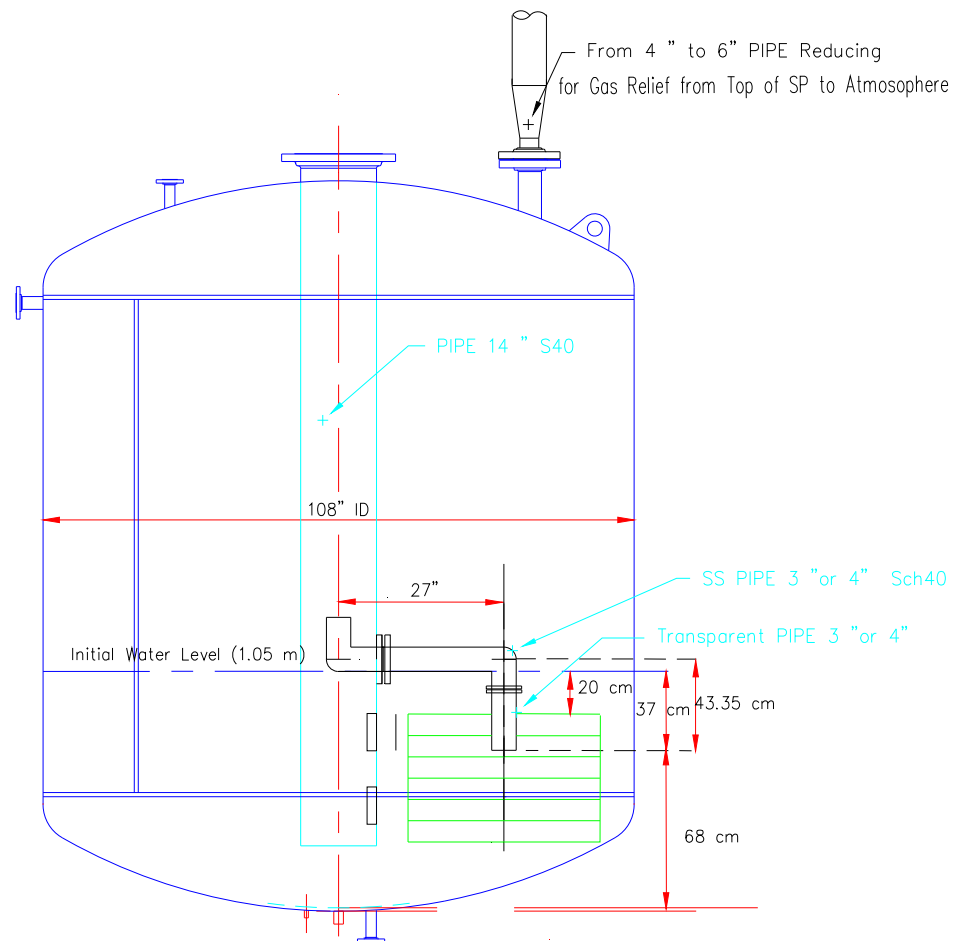


Figure 3.5 Side View of SP with Modification for Transient Tests.

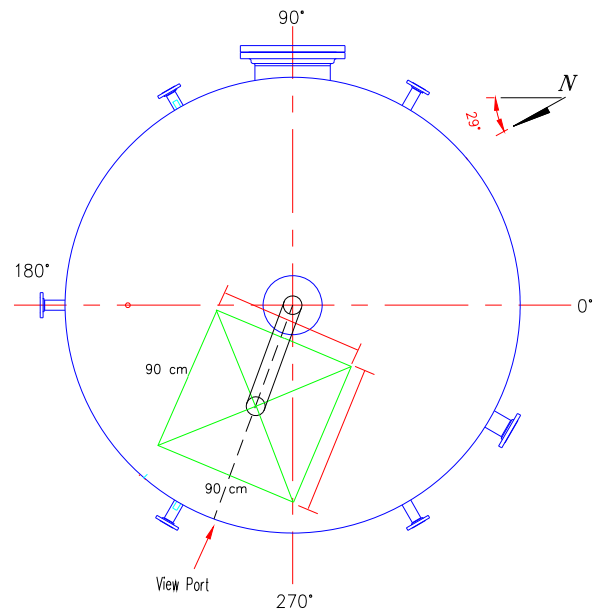


Figure 3.6 Top View of SP with Modification for Transient Tests.

## CHAPTER 4. INSTRUMENTATIONS

In the experimental facility, several major instruments need to be installed to obtain the required information such as the void fraction, bubble velocity, bubble size (chord length) and inlet flow condition.

The chapter of instrumentations for the tests is divided into two sections: local instruments inside the SP and instruments outside the SP. The local instruments in the SP are the conductivity probes on the supporting cage with the pressure gauges, thermocouples and oxygen concentration measurement. The instruments outside the SP are the vortex flow meters, thermocouples, and pressure gauges in the air injection line for steady-state tests. The pressure gauges, thermocouples in the DW, and vortex flow meters in steam lines from the RPV to the DW will be classified as instruments outside the SP for transients tests.

### 4.1. Local Instruments in SP

#### 4.1.1. Conductivity Probes and Supporting Cage

There are two types of conductivity probes used in this experiment. One is the single-sensor conductivity probe and the other is the double-sensor conductivity probe. The single-sensor conductivity probe is to measure the local void fraction while the double-sensor conductivity probe is to measure simultaneously both of the local void fraction, bubble velocity and chord length.

As shown in Figure 4.1, the single-sensor conductivity probe consists of an electrode which is made by teflon coated stainless steel wire with 0.024-inch diameter. The teflon coating on the tip of the wire will be ground out to a sharp edge with the length of 0.05-inch. To protect any scratches to the wire that can create a disturbance of signal, a heat shrink tube will be applied to cover the stainless steel wire. The probes will be installed on the stainless steel tube with 0.5-inch diameter through conax fittings.

The design of the double-sensor conductivity probe is similar to the single-sensor conductivity probe. The main difference between the single- and double-sensor conductivity probe design is the number of stainless steel wires in the probe. As shown in Figure 4.2, the double-sensor conductivity probe consists of two electrodes which have the same diameter as the single-sensor conductivity probe. Additionally, to measure the bubble velocity, the two electrodes will be arranged with a height difference around 0.15 inch.

The stainless steel wire will be connected with fine gauge insulated wire to carry the voltage signals to an electronic circuit and Data Acquisition System (DAS). Finally, The electric signals will be converted to the void fraction, bubble velocity and chord length information [7,8].

The arrangement in the measurement points of conductivity probes on the supporting cage is displayed in Figure 4.3. The 54 single-sensor and 24 double-sensor conductivity probes are mounted systematically on the supporting cage which has a cubic shape in size 0.9 m×0.9 m×1.2 m. The probes configuration has 6 axial levels (Level A to F) and 7 radial positions from the center of downcomer pipe in a cross-shaped pattern. The probe locations are designed based on the size of the bubble plume obtained by the CFD simulation results. The 6 axial levels of probes will be adjustable according to the bubble plume size observed from the actual experiments.

In each level of probes, one fourth of the cross-shaped tubes are mounted with 3 single-sensor and 3 double sensor conductivity probes to measure detailed void fraction and bubble velocity while others are mounted with 3 single-conductivity probes to check the symmetry of the void fraction in the bubble plume.

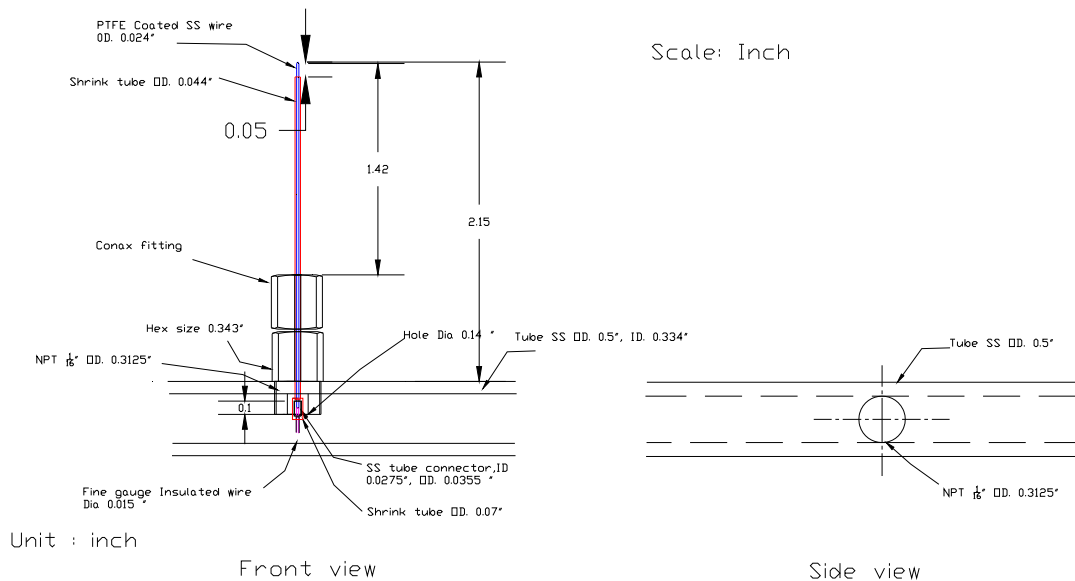


Figure 4.1 Design of Single-Sensor Conductivity Probe.

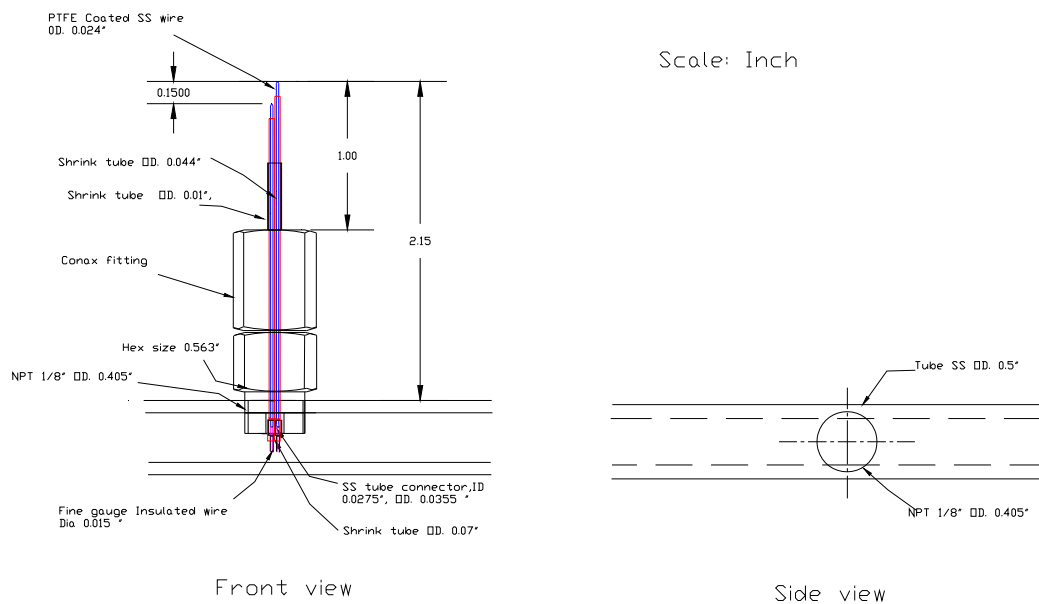


Figure 4.2 Design of Double-Sensor Conductivity Probe.

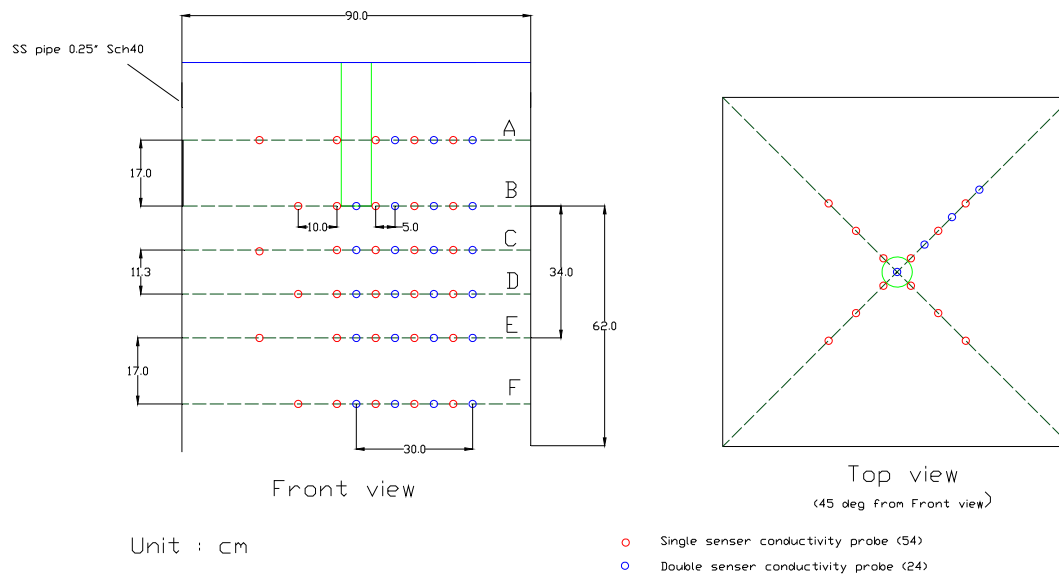


Figure 4.3 Configuration of Single-Sensor and Double-Sensor Conductivity Probes on Supporting Cage.

#### 4.1.2. Single-Sensor Conductivity Probes in Downcomer

In order to estimate the water column velocity during the vent clearing period, the 5 single-sensor conductivity probes will be installed on the side of the transparent lexan pipe at the 5 axial levels from the exit of downcomer to the water level. The arrangement of the probes is shown in Figure 4.4. It is noted that the highest probe located at the water level in the SP will be used to determine the initial water level in the downcomer. Also, the lowest probe positioned at the exit of downcomer can provide the information of the vent clearing time.

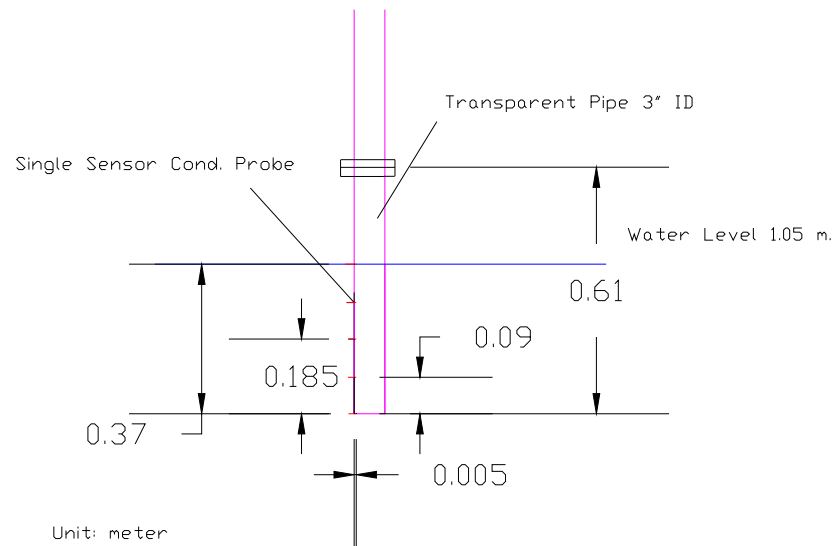


Figure 4.4 Configuration of the Single-Sensor Conductivity Probes in Downcomer.

#### 4.1.3. Thermocouples on Cage

The 15 T-type thermocouples will be installed on the cage around the exit of downcomer to investigate the temperature distribution in the SP when steam is released from the DW to the SP through the downcomer. The measurable range of the thermocouples is  $-200\sim 250$  °C.

#### 4.1.4. Pressure, Temperature and Water Level Measurement in SP

As for the absolute pressure, temperature and water level measurements, some of the existing instruments in the PUMA-E facility will be used in the experiment. The location of four thermocouples (TE-SP-02, 04, 08, 10), two absolute pressure gauges (PT-SP-01, 02) and two differential pressure gauges (LT-SP-01, 02) for water level measurement are shown in Figure 4.5. A new differential pressure gauge (PT-AL-03) between the air line connected to the SRV line and the gas space in the SP will be installed to estimate the water level in the downcomer.

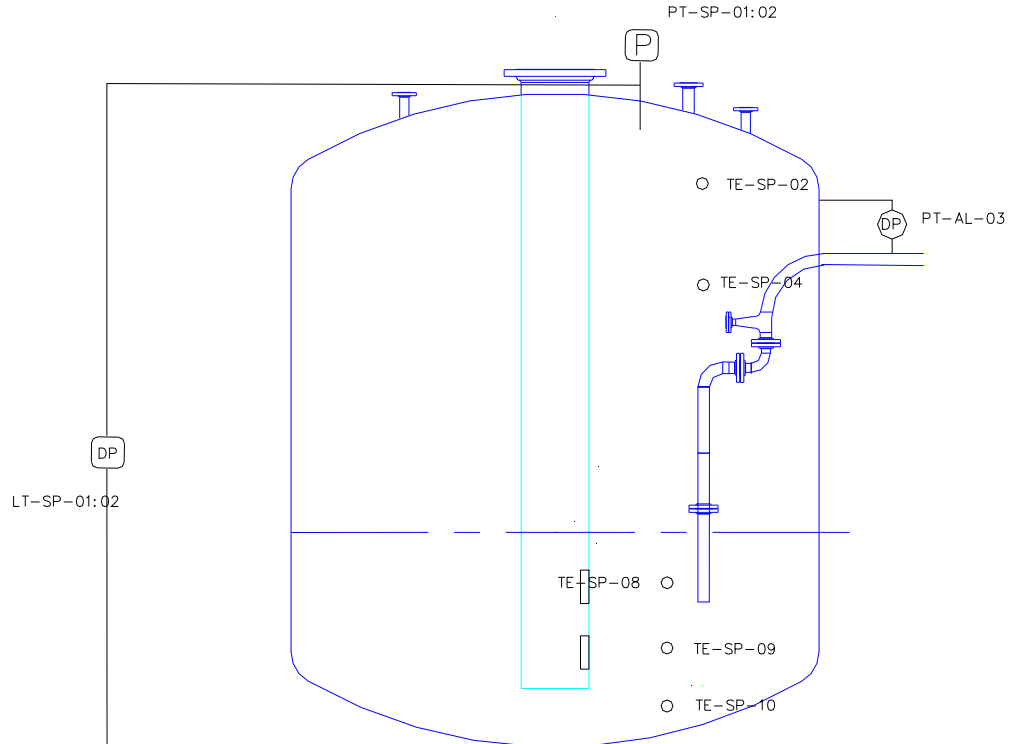


Figure 4.5 Locations of Pressure and Water Level Measurement in SP.

#### 4.1.5. Air Concentration Measurement

One oxygen analyzer used in the PUMA-E facility will be utilized to measure the air concentration at the inlet of the downcomer section for the transient tests. Figure 4.6 shows the location of sampling line. The oxygen sensor is the Thermox RM CEM O2/IQ; Extractive Zirconium Oxide Oxygen Analyzer manufactured by AMETEK. This transducer measures oxygen concentrations over a range of 0 ~ 21%, which represents the air concentration with a range of 0 ~ 100%. The transducer accuracy is  $\pm 0.05\%$  O<sub>2</sub> concentration or  $\pm 0.75\%$  of reading, whichever is greater. Since the upper range limit is 21%, the accuracy was chosen to be  $\pm 0.16\%$  O<sub>2</sub>, and this is assumed to be a bias uncertainty. For this range of oxygen concentrations, the EXP-16 multiplexer linearity is  $\pm 0.003\%$  O<sub>2</sub> (bias) and the peak-to-peak noise is  $\pm 0.029\%$  O<sub>2</sub>. The overall uncertainty for this measurement, including both bias and precision components for the transducer and electronics, is  $\pm 0.2\%$  O<sub>2</sub>.

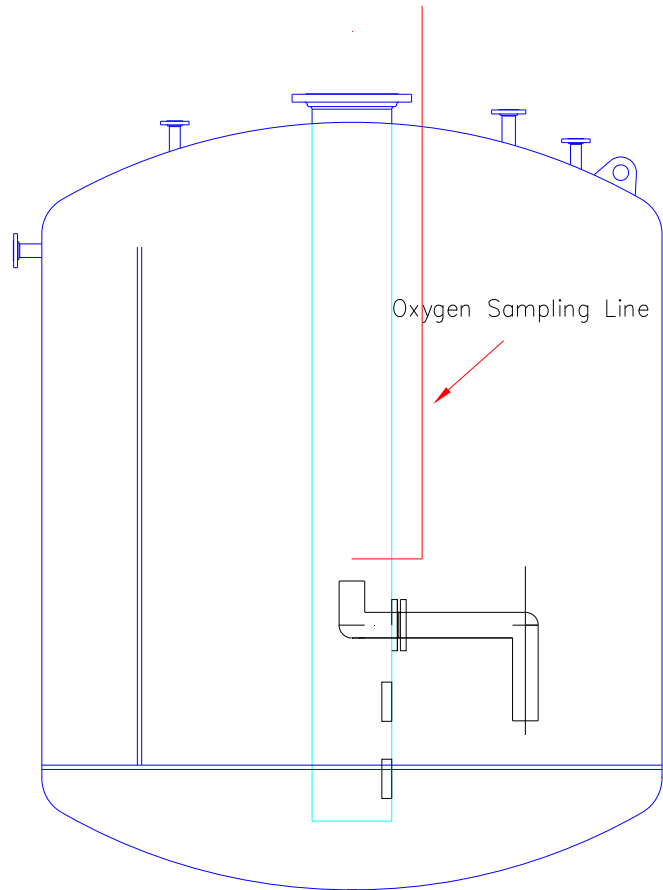


Figure 4.6 Oxygen Sampling Line inside SP.

## 4.2. Instruments outside SP

### 4.2.1. Instruments in Air Injection Line

#### 4.2.1.1. Vortex Flow Meter

Two Foxboro vortex flowmeters will be installed on the parallel 2-inch and ¾-inch pipe lines to measure air flows for low and high flow conditions. The vortex flowmeter works on the principle that a disturbance in the flow field generates vortices which are proportional to the flow rate. Therefore, the flow can be measured by counting the number of vortices per unit time. These flow meters measure gas velocities in the range of 1.5 m/s to 120 m/s at atmospheric conditions. There is an overall uncertainty of  $\pm 1\%$  of the upper range value. The output from the vortex flow meter is a 4 to 20 mA signal.

#### 4.2.1.2. Pressure and Temperature

Pressure and temperature at the air injection line are measured by pressure transducers and thermocouples, respectively. Temperature is measured by sheathed K-type thermocouples. The thermocouple signals, in mV, are converted directly to engineering units by the DAS software. The range of the thermocouples is -200~1250 °C and the uncertainty is  $\pm 2$  °C.

The PUMA-E facility uses pressure transducers manufactured by Honeywell for all pressure and differential pressure measurements. These transducers are designed to measure pressure over a specific range.

#### 4.2.2. High-Speed Video Movie Camera

A high-speed camera (Kodak Motion Corder Analyzer), which can take an image at the recording speed of 10,000 frames per second, is available at PUMA-E facility. For this study, up to 500 frames per second shall be sufficient. It can be used to visualize the transient venting phenomena of gas plume around the exit of downcomer. Captured digital images can be transferred to a computer. The camera will be installed at the viewport on the side of SP as shown in Figure 3.6.

#### 4.2.3. Existing Instruments in PUMA-E Facility

##### 4.2.3.1. Flow Measurement

Foxboro vortex flowmeters installed to measure steam flow released from the RPV to the DW on the MSL and DPV lines. According to test condition, the line between RPV and DW will be determined.

##### 4.2.3.2. Pressure and Temperature Measurement in DW

The gas space pressure in the DW is measured with the existing pressure transducers (PT-DW-01,02). The DW water level is measured by two differential pressure transducers (LT-DW-01,02). Several thermocouples are placed inside the DW to measure the gas temperatures. Figure 4.7 shows the pressure and level transmitter locations in the DW.

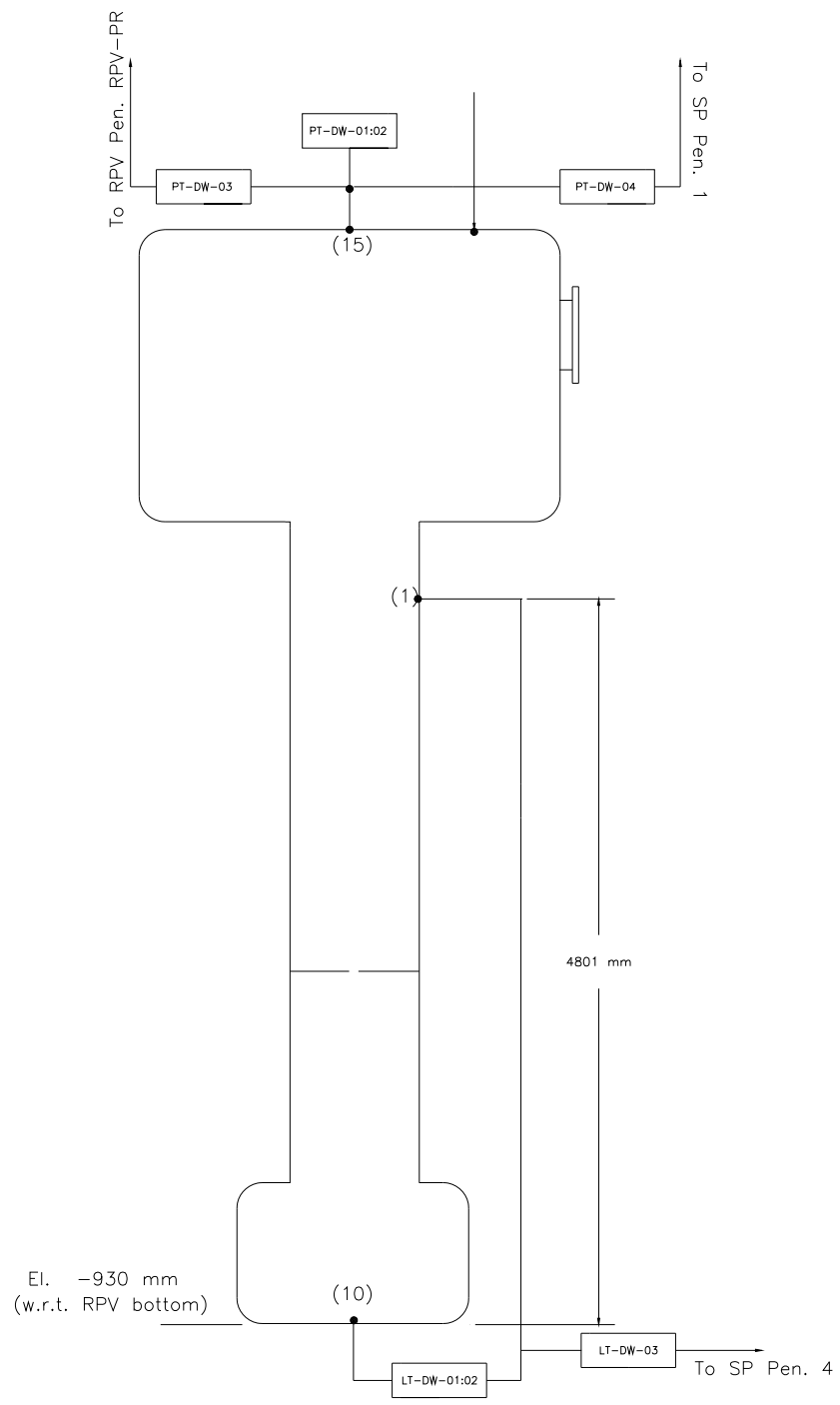


Figure 4.7 DW Pressure and Level Transmitter Locations.

## CHAPTER 5. SUMMARY AND FUTURE WORK

This report is prepared by Thermal-Hydraulics and Reactor Safety Laboratory (TRSL) at Purdue University for Task 6: *Suppression Pool Void Distribution During Blowdown* which is supported by the U.S. Nuclear Regulatory Commission. In this report, the scaling consideration of the MARK-I to the PUMA-E facility for the venting phenomena of the SP during the blowdown are explained and preliminary demonstration of the scaling approach is presented with a CFD simulation. The PUMA-E facility modifications based on the scaling for the steady-state and transient experiments are proposed. The instrumentation that will be used in the both experiments is described.

The next steps of Task 6 will be the facility modification and installation of instruments for the steady-state tests based on the scaling and designs proposed in this report. The calibration for instruments and shake-down test for steady-state tests will be performed right after the finishing of facility modification and instruments installation.

## LIST OF REFERENCES

1. J. Foster, M. Reisi Fard, J. Kauffman, GSI-193 BWR ECCS Suction Concerns, NUREG-0933, June 2008.
2. Mark I containment Short Term Program – Safety Evaluation Report, NUREG-0408, December, 1977.
3. M. Ishii, S. T. Revankar, R. Dowlati, et al., “Scientific Design of Purdue University Multi-Dimensional Integral Test Assembly (PUMA) for GE SBWR,” PU-NE-94/1, NUREG/CR-6309, 1996.
4. Mark I containment Long Term Program – Safety Evaluation Report, NUREG-0661, December, 1980.
5. General Characteristics of BWR LWR for GSI-193 Technical Assessment, U.S. NRC, 2009 (Personal communication).
6. A. Velazquez, et al., Comments on the Proposal for Task 6: Suppression Pool Void Distribution during Blow-down. U.S. NRC, 2009 (Personal communication).
7. T. Hibiki, S. Hogsett, M. Ishii, “Local Measurement of Interfacial Area, Interfacial Velocity and Liquid Turbulence in Two-Phase Flow,” Nucl. Eng. Des. 184 (1998) 287-304.
8. S.T. Revankar, M. Ishii, et al., “Instrumentation for the PUMA Integral Test Facility,” PU-NE-98-3, NUREG/CR-5578, 1999.